CHALMERS

An Introduction to Turbulence Models

Lars Davidson, http://www.tfd.chalmers.se/~lada

Department of Thermo and Fluid Dynamics
CHALMERS UNIVERSITY OF TECHNOLOGY
Göteborg, Sweden, February 24, 2011

Contents

Nomenclature

Latin Symbols

c_1, c_2, c_s	constants in the Reynolds stress model
c_1', c_2'	constants in the Reynolds stress model
$c_{\varepsilon 1}, c_{\varepsilon 2}$	constants in the modelled ε equation
$c_{\omega 1}, c_{\omega 2}$	constants in the modelled ω equation
c_μ	constant in turbulence model
E	energy (see Eq. 1.8); constant in wall functions (see Eq. 3.4)
f	damping function in pressure strain tensor
k	turbulent kinetic energy $(\equiv \frac{1}{2}\overline{u_i u_i})$
U	instantaneous (or laminar) velocity in x-direction
U_i	instantaneous (or laminar) velocity in x_i-direction
$\bar{U}$	time-averaged velocity in x-direction
$\bar{U}_i$	time-averaged velocity in x_i-direction
$\overline{uv}, \overline{uw}$	shear stresses
u	fluctuating velocity in x-direction
$\overline{u^2}$	normal stress in the x-direction
u_i	fluctuating velocity in x_i-direction
$\overline{u_i u_j}$	Reynolds stress tensor
V	instantaneous (or laminar) velocity in y-direction
$\bar{V}$	time-averaged velocity in y-direction
v	fluctuating (or laminar) velocity in y-direction
$\overline{v^2}$	normal stress in the y-direction
$\overline{vw}$	shear stress
W	instantaneous (or laminar) velocity in z-direction
$\bar{W}$	time-averaged velocity in z-direction
w	fluctuating velocity in z-direction
$\overline{w^2}$	normal stress in the z-direction

Greek Symbols

δ	boundary layer thickness; half channel height
ε	dissipation
κ	wave number; von Karman constant $(= 0.41)$
μ	dynamic viscosity
μ_t	dynamic turbulent viscosity
ν	kinematic viscosity
ν_t	kinematic turbulent viscosity
Ω_i	instantaneous (or laminar) vorticity component in x_i-direction

$\bar{\Omega}_i$	time-averaged vorticity component in x_i-direction
ω	specific dissipation ($\propto \varepsilon/k$)
ω_i	fluctuating vorticity component in x_i-direction
σ_Φ	turbulent Prandtl number for variable Φ
τ_{lam}	laminar shear stress
τ_{tot}	total shear stress
τ_{turb}	turbulent shear stress

Subscript

C	centerline
w	wall

1 Turbulence

1.1 Introduction

Almost all fluid flow which we encounter in daily life is turbulent. Typical examples are flow around (as well as *in*) cars, aeroplanes and buildings. The boundary layers and the wakes around and after bluff bodies such as cars, aeroplanes and buildings are turbulent. Also the flow and combustion in engines, both in piston engines and gas turbines and combustors, are highly turbulent. Air movements in rooms are also turbulent, at least along the walls where wall-jets are formed. Hence, when we compute fluid flow it will most likely be turbulent.

In turbulent flow we usually divide the variables in one time-averaged part $\bar{U}$, which is independent of time (when the mean flow is steady), and one fluctuating part u so that $U = \bar{U} + u$.

There is no definition on turbulent flow, but it has a number of characteristic features (see Tennekes & Lumley [43]) such as:

I. Irregularity. Turbulent flow is irregular, random and chaotic. The flow consists of a spectrum of different scales (eddy sizes) where largest eddies are of the order of the flow geometry (i.e. boundary layer thickness, jet width, etc). At the other end of the spectra we have the smallest eddies which are by viscous forces (stresses) dissipated into internal energy. Even though turbulence is chaotic it is deterministic and is described by the Navier-Stokes equations.

II. Diffusivity. In turbulent flow the diffusivity increases. This means that the spreading rate of boundary layers, jets, etc. increases as the flow becomes turbulent. The turbulence increases the exchange of momentum in e.g. boundary layers and reduces or delays thereby separation at bluff bodies such as cylinders, airfoils and cars. The increased diffusivity also increases the resistance (wall friction) in internal flows such as in channels and pipes.

III. Large Reynolds Numbers. Turbulent flow occurs at high Reynolds number. For example, the transition to turbulent flow in pipes occurs that $Re_D \simeq 2300$, and in boundary layers at $Re_x \simeq 100000$.

IV. Three-Dimensional. Turbulent flow is always three-dimensional. However, when the equations are time averaged we can treat the flow as two-dimensional.

V. Dissipation. Turbulent flow is dissipative, which means that kinetic energy in the small (dissipative) eddies are transformed into internal energy. The small eddies receive the kinetic energy from slightly larger eddies. The slightly larger eddies receive their energy from even larger eddies and so on. The largest eddies extract their energy from the mean flow. This process of transferred energy from the largest turbulent scales (eddies) to the smallest is called *cascade process*.

VI. Continuum. Even though we have small turbulent scales in the flow they are much larger than the molecular scale and we can treat the flow as a continuum.

1.2 Turbulent Scales

As mentioned above there are a wide range of scales in turbulent flow. The larger scales are of the order of the flow geometry, for example the boundary layer thickness, with length scale ℓ and velocity scale $\mathcal{U}$. These scales extract kinetic energy from the mean flow which has a time scale comparable to the large scales, i.e.

$$\frac{\partial \bar{U}}{\partial y} = \mathcal{O}(\mathcal{T}^{-1}) = \mathcal{O}(\mathcal{U}/\ell)$$

The kinetic energy of the large scales is lost to slightly smaller scales with which the large scales interact. Through the *cascade process* the kinetic energy is in this way transferred from the largest scale to smaller scales. At the smallest scales the frictional forces (viscous stresses) become too large and the kinetic energy is transformed (dissipated) into internal energy. The dissipation is denoted by ε which is energy per unit time and unit mass ($\varepsilon = [m^2/s^3]$). The dissipation is proportional to the kinematic viscosity ν times the fluctuating velocity gradient up to the power of two (see Section 2.4.1). The friction forces exist of course at all scales, but they are larger the smaller the eddies. Thus it is not quite true that eddies which receive their kinetic energy from slightly larger scales give away all of that the slightly smaller scales but a small fraction is dissipated. However it is assumed that most of the energy (say 90 %) that goes into the large scales is finally dissipated at the smallest (dissipative) scales.

The smallest scales where dissipation occurs are called the Kolmogorov scales: the velocity scale υ, the length scale η and the time scale τ. We assume that these scales are determined by viscosity ν and dissipation ε. Since the kinetic energy is destroyed by viscous forces it is natural to assume that viscosity plays a part in determining these scales; the larger viscosity, the larger scales. The amount of energy that is to be dissipated is ε. The more energy that is to be transformed from kinetic energy to internal energy, the larger the velocity gradients must be. Having assumed that the dissipative scales are determined by viscosity and dissipation, we can express υ, η and τ in ν and ε using dimensional analysis. We write

$$\begin{aligned} \upsilon &= \nu^a & \varepsilon^b \\ [m/s] &= [m^2/s] & [m^2/s^3] \end{aligned} \tag{1.1}$$

where below each variable its dimensions are given. The dimensions of the left-hand and the right-hand side must be the same. We get two equations,

one for meters $[m]$

$$1 = 2a + 2b, \tag{1.2}$$

and one for seconds $[s]$

$$-1 = -a - 3b, \tag{1.3}$$

which gives $a = b = 1/4$. In the same way we obtain the expressions for η and τ so that

$$\upsilon = (\nu\varepsilon)^{1/4}, \ \eta = \left(\frac{\nu^3}{\varepsilon}\right)^{1/4}, \ \tau = \left(\frac{\nu}{\varepsilon}\right)^{1/2} \tag{1.4}$$

1.3 Vorticity/Velocity Gradient Interaction

The interaction between vorticity and velocity gradients is an essential ingredient to create and maintain turbulence. Disturbances are amplified – the actual process depending on type of flow – and these disturbances, which still are laminar and organized and well defined in terms of physical orientation and frequency are turned into chaotic, three-dimensional, random fluctuations, i.e. turbulent flow by interaction between the vorticity vector and the velocity gradients. Two idealized phenomena in this interaction process can be identified: vortex stretching and vortex tilting.

In order to gain some insight in vortex shedding we will study an idealized, inviscid (viscosity equals to zero) case. The equation for instantaneous vorticity ($\Omega_i = \bar{\Omega}_i + \omega_i$) reads [43, 33, 46]

$$\begin{aligned} U_j\Omega_{i,j} &= \Omega_j U_{i,j} + \nu\Omega_{i,jj} \\ \Omega_i &= \epsilon_{ijk}U_{k,j} \end{aligned} \tag{1.5}$$

where ϵ_{ijk} is the Levi-Civita tensor (it is $+1$ if i, j k are in cyclic order, -1 if i, j k are in anti-cyclic order, and 0 if any two of i, j k are equal), and where $(.)_{,j}$ denotes derivation with respect to x_j. We see that this equation is not an ordinary convection-diffusion equation but is has an additional term on the right-hand side which represents amplification and rotation/tilting of the vorticity lines. If we write it term-by-term it reads

$$\begin{aligned} \Omega_1 U_{1,1} + \Omega_2 U_{1,2} + \Omega_3 U_{1,3} \\ \Omega_1 U_{2,1} + \Omega_2 U_{2,2} + \Omega_3 U_{2,3} \\ \Omega_1 U_{3,1} + \Omega_2 U_{3,2} + \Omega_3 U_{3,3} \end{aligned} \tag{1.6}$$

The diagonal terms in this matrix represent *vortex stretching*. Imagine a slender, cylindrical fluid element which vorticity $\boldsymbol{\Omega}$. We introduce a cylindrical coordinate system with the x_1-axis as the cylinder axis and x_2 as the **Vortex stretching**

Figure 1.1: Vortex stretching.

radial coordinate (see Fig. 1.1) so that $\mathbf{\Omega} = (\Omega_1, 0, 0)$. A positive $U_{1,1}$ will stretch the cylinder. From the continuity equation

$$U_{1,1} + \frac{1}{r}(rU_2)_{,2} = 0$$

we find that the radial derivative of the radial velocity U_2 must be negative, i.e. the radius of the cylinder will decrease. We have neglected the viscosity since viscous diffusion at high Reynolds number is much smaller than the turbulent one and since viscous dissipation occurs at small scales (see p. 6). Thus there are no viscous stresses acting on the cylindrical fluid element surface which means that the rotation momentum

$$r^2\Omega \tag{1.7}$$

remains constant as the radius of the fluid element decreases (note that also the circulation $\Gamma \propto \Omega r^2$ is constant). Equation 1.7 shows that the vorticity increases as the radius decreases. We see that a stretching/compressing will decrease/increase the radius of a slender fluid element and increase/decrease its vorticity component aligned with the element. This process will affect the vorticity components in the other two coordinate directions.

The off-diagonal terms in Eq. 1.6 represent *vortex tilting*. Again, take a **Vortex** slender fluid element with its axis aligned with the x_2 axis, Fig. 1.2. The ve- **tilting** locity gradient $U_{1,2}$ will tilt the fluid element so that it rotates in clock-wise direction. The second term $\Omega_2 U_{1,2}$ in line one in Eq. 1.6 gives a contribution to Ω_1.

Vortex stretching and vortex tilting thus qualitatively explains how interaction between vorticity and velocity gradient create vorticity in all three coordinate directions from a disturbance which initially was well defined in one coordinate direction. Once this process has started it continues, because vorticity generated by vortex stretching and vortex tilting interacts with the velocity field and creates further vorticity and so on. The vorticity and velocity field becomes chaotic and random: turbulence has been created. The turbulence is also maintained by these processes.

From the discussion above we can now understand why turbulence always must be three-dimensional (Item IV on p. 5). If the instantaneous flow is two-dimensional we find that all interaction terms between vorticity and velocity gradients in Eq. 1.6 vanish. For example if $U_3 \equiv 0$ and all derivatives with respect to x_3 are zero. If $U_3 \equiv 0$ the third line in Eq. 1.6 vanishes, and if $U_{i,3} \equiv 0$ the third column in Eq. 1.6 disappears. Finally, the
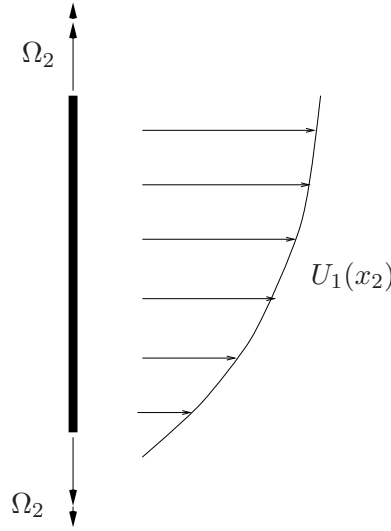
Figure 1.2: Vortex tilting.

remaining terms in Eq. 1.6 will also be zero since

$$\Omega_1 = U_{3,2} - U_{2,3} \equiv 0$$
$$\Omega_2 = U_{1,3} - U_{3,1} \equiv 0.$$

The interaction between vorticity and velocity gradients will, on average, create smaller and smaller scales. Whereas the large scales which interact with the mean flow have an orientation imposed by the mean flow the small scales will not remember the structure and orientation of the large scales. Thus the small scales will be *isotropic*, i.e independent of direction.

1.4 Energy spectrum

The turbulent scales are distributed over a range of scales which extends from the largest scales which interact with the mean flow to the smallest scales where dissipation occurs. In wave number space the energy of eddies from κ to $\kappa + d\kappa$ can be expressed as

$$E(\kappa)d\kappa \tag{1.8}$$

where Eq. 1.8 expresses the contribution from the scales with wave number between κ and $\kappa + d\kappa$ to the turbulent kinetic energy k. The dimension of wave number is one over length; thus we can think of wave number as proportional to the inverse of an eddy's radius, i.e $\kappa \propto 1/r$. The total turbulent kinetic energy is obtained by integrating over the whole wave number space i.e.

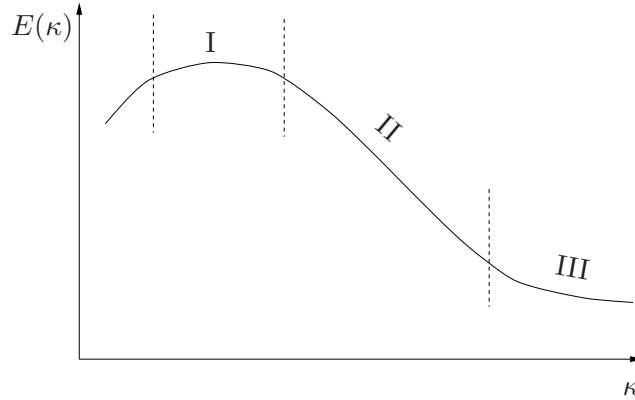$$k = \int_0^\infty E(\kappa)d\kappa \tag{1.9}$$

Figure 1.3: Spectrum for k. I: Range for the large, energy containing eddies. II: the inertial subrange. III: Range for small, isotropic scales.

The kinetic energy is the sum of the kinetic energy of the three fluctuating velocity components, i.e.

$$k = \frac{1}{2}\left(\overline{u^2} + \overline{v^2} + \overline{w^2}\right) = \frac{1}{2}\overline{u_i u_i} \tag{1.10}$$

The spectrum of E is shown in Fig. 1.3. We find region I, II and III which correspond to:

I. In the region we have the large eddies which carry most of the energy. These eddies interact with the mean flow and extract energy from the mean flow. Their energy is past on to slightly smaller scales. The eddies' velocity and length scales are $\mathcal{U}$ and ℓ, respectively.

III. Dissipation range. The eddies are small and isotropic and it is here that the dissipation occurs. The scales of the eddies are described by the Kolmogorov scales (see Eq. 1.4)

II. Inertial subrange. The existence of this region requires that the Reynolds number is high (fully turbulent flow). The eddies in this region represent the mid-region. This region is a "transport" region in the cascade process. Energy per time unit (ε) is coming from the large eddies at the lower part of this range and is given off to the dissipation range at the higher part. The eddies in this region are independent of both the large, energy containing eddies and the eddies in the dissipation range. One can argue that the eddies in this region should be characterized by the flow of energy (ε) and the size of the eddies $1/\kappa$. Dimensional reasoning gives

$$E(\kappa) = const. \, \varepsilon^{\frac{2}{3}} \kappa^{-\frac{5}{3}} \tag{1.11}$$

This is a very important law (Kolmogorov spectrum law or the $-5/3$ law) which states that, if the flow is fully turbulent (high Reynolds

number), the energy spectra should exhibit a $-5/3$-decay. This often used in experiment and $\underline{L}$arge $\underline{E}$ddy $\underline{S}$imulations (LES) and $\underline{D}$irect $\underline{N}$umerical $\underline{S}$imulations (DNS) to verify that the flow is fully turbulent.

As explained on p. 6 (cascade process) the energy dissipated at the small scales can be estimated using the large scales $\mathcal{U}$ and ℓ. The energy at the large scales lose their energy during a time proportional to $\ell/\mathcal{U}$, which gives

$$\varepsilon = \mathcal{O}\left(\frac{\mathcal{U}^2}{\ell/\mathcal{U}}\right) = \mathcal{O}\left(\frac{\mathcal{U}^3}{\ell}\right) \tag{1.12}$$

2 Turbulence Models

2.1 Introduction

When the flow is turbulent it is preferable to decompose the instantaneous variables (for example velocity components and pressure) into a mean value and a fluctuating value, i.e.

$$U_i = \bar{U}_i + u_i$$
$$P = \bar{P} + p. \tag{2.1}$$

One reason why we decompose the variables is that when we measure flow quantities we are usually interested in the mean values rather that the time histories. Another reason is that when we want to solve the Navier-Stokes equation numerically it would require a very fine grid to resolve all turbulent scales and it would also require a fine resolution in time (turbulent flow is always unsteady).

The continuity equation and the Navier-Stokes equation read

$$\frac{\partial \rho}{\partial t} + (\rho U_i)_{,i} = 0 \tag{2.2}$$

$$\frac{\partial \rho U_i}{\partial t} + (\rho U_i U_j)_{,j} = -P_{,i} + \left[\mu \left(U_{i,j} + U_{j,i} - \frac{2}{3} \delta_{ij} U_{k,k} \right) \right]_{,j} \tag{2.3}$$

where $(.)_{,j}$ denotes derivation with respect to x_j. Since we are dealing with incompressible flow (i.e low Mach number) the dilatation term on the right-hand side of Eq. 2.3 is neglected so that

$$\frac{\partial \rho U_i}{\partial t} + (\rho U_i U_j)_{,j} = -P_{,i} + [\mu(U_{i,j} + U_{j,i})]_{,j}. \tag{2.4}$$

Note that we here use the term "incompressible" in the sense that density is independent of pressure ($\partial P/\partial \rho = 0$) , but it does not mean that density is constant; it can be dependent on for example temperature or concentration.

Inserting Eq. 2.1 into the continuity equation (2.2) and the Navier-Stokes equation (2.4) we obtain the *time averaged* continuity equation and Navier-Stokes equation

$$\frac{\partial \rho}{\partial t} + (\rho \bar{U}_i)_{,i} = 0 \tag{2.5}$$

$$\frac{\partial \rho \bar{U}_i}{\partial t} + \left(\rho \bar{U}_i \bar{U}_j \right)_{,j} = -\bar{P}_{,i} + \left[\mu(\bar{U}_{i,j} + \bar{U}_{j,i}) - \rho \overline{u_i u_j} \right]_{,j}. \tag{2.6}$$

A new term $\overline{u_i u_j}$ appears on the right-hand side of Eq. 2.6 which is called the *Reynolds stress tensor*. The tensor is symmetric (for example $\overline{u_1 u_2} = \overline{u_2 u_1}$). It represents correlations between fluctuating velocities. It is an additional stress term due to turbulence (fluctuating velocities) and it is unknown. We need a model for $\overline{u_i u_j}$ to close the equation system in Eq. 2.6.
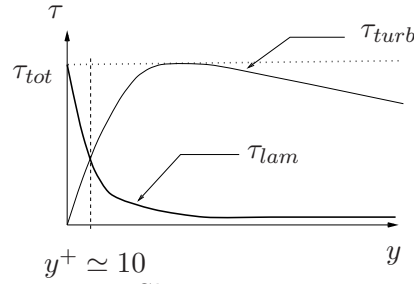
Figure 2.1: Shear stress near a wall.

This is called the *closure problem*: the number of unknowns (ten: three veloc- **closure** ity components, pressure, six stresses) is larger than the number of equa- **problem** tions (four: the continuity equation and three components of the Navier-Stokes equations).

For steady, two-dimensional boundary-layer type of flow (i.e. boundary layers along a flat plate, channel flow, pipe flow, jet and wake flow, etc.) where

$$\bar{V} \ll \bar{U}, \ \frac{\partial}{\partial x} \ll \frac{\partial}{\partial y} \tag{2.7}$$

Eq. 2.6 reads

$$\frac{\partial \rho \bar{U} \bar{U}}{\partial x} + \frac{\partial \rho \bar{V} \bar{U}}{\partial y} \ = \ -\frac{\partial \bar{P}}{\partial x} + \frac{\partial}{\partial y} \underbrace{\left[\mu \frac{\partial \bar{U}}{\partial y} - \rho \overline{uv} \right]}_{\tau_{tot}}. \tag{2.8}$$

$x = x_1$ denotes streamwise coordinate, and $y = x_2$ coordinate normal to the flow. Often the pressure gradient $\partial \bar{P}/\partial x$ is zero.

To the viscous shear stress $\mu \partial \bar{U}/\partial y$ on the right-hand side of Eq. 2.8 **shear** appears an additional *turbulent* one, a turbulent shear stress. The total shear **stress** stress is thus

$$\tau_{tot} = \mu \frac{\partial \bar{U}}{\partial y} - \rho \overline{uv}$$

In the wall region (the viscous sublayer, the buffert layer and the logarithmic layer) the total shear stress is approximately constant and equal to the wall shear stress τ_w, see Fig. 2.1. Note that the total shear stress is constant only close to the wall; further away from the wall it decreases (in fully developed channel flow it decreases linearly by the distance form the wall). At the wall the turbulent shear stress vanishes as $u = v = 0$, and the viscous shear stress attains its wall-stress value $\tau_w = \rho u_*^2$. As we go away from the wall the viscous stress decreases and turbulent one increases and at $y^+ \simeq 10$ they are approximately equal. In the logarithmic layer the viscous stress is negligible compared to the turbulent stress.

In boundary-layer type of flow the turbulent shear stress and the velocity gradient $\partial \bar{U}/\partial y$ have nearly always opposite sign (for a wall jet this
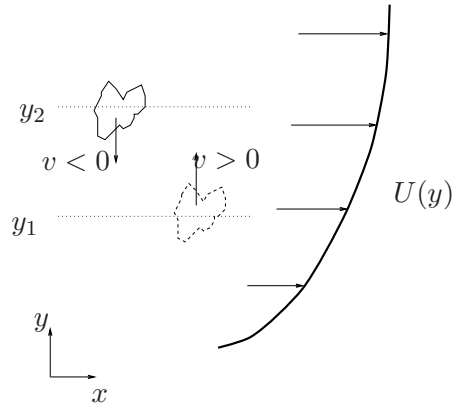
Figure 2.2: Sign of the turbulent shear stress $-\rho\overline{uv}$ in a boundary layer.

is not the case close to the wall). To get a physical picture of this let us study the flow in a boundary layer, see Fig. 2.2. A fluid particle is moving downwards (particle drawn with solid line) from y_2 to y_1 with (the turbulent fluctuating) velocity v. At its new location the U velocity is in average smaller than at its old, i.e. $\bar{U}(y_1) < \bar{U}(y_2)$. This means that when the particle at y_2 (which has streamwise velocity $U(y_2)$) comes down to y_1 (where the streamwise velocity is $U(y_1)$) is has an excess of streamwise velocity compared to its new environment at y_1. Thus the streamwise fluctuation is positive, i.e. $u > 0$ and the correlation between u and v is negative ($uv < 0$).

If we look at the other particle (dashed line in Fig. 2.2) we reach the same conclusion. The particle is moving upwards ($v > 0$), and it is bringing a deficit in U so that $u < 0$. Thus, again, $uv < 0$. If we study this flow for a long time and average over time we get $\overline{uv} < 0$. If we change the sign of the velocity gradient so that $\partial\bar{U}/\partial y < 0$ we will find that the sign of $\overline{uv}$ also changes.

Above we have used physical reasoning to show the the signs of $\overline{uv}$ and $\partial\bar{U}/\partial y$ are opposite. This can also be found by looking at the production term in the transport equation of the Reynolds stresses (see Section 5). In cases where the shear stress and the velocity gradient have the same sign (for example, in a wall jet) this means that there are other terms in the transport equation which are more important than the production term.

There are different levels of approximations involved when closing the equation system in Eq. 2.6.

I. Algebraic models. An algebraic equation is used to compute a turbulent viscosity, often called *eddy* viscosity. The Reynolds stress tensor is then computed using an assumption which relates the Reynolds stress tensor to the velocity gradients and the turbulent viscosity. This assumption is called the *Boussinesq assumption*. Models which are based on a turbulent (eddy) viscosity are called *eddy viscosity* mod-

els.

II. **One-equation models.** In these models a transport equation is solved for a turbulent quantity (usually the turbulent kinetic energy) and a second turbulent quantity (usually a turbulent length scale) is obtained from an algebraic expression. The turbulent viscosity is calculated from Boussinesq assumption.

III. **Two-equation models.** These models fall into the class of eddy viscosity models. Two transport equations are derived which describe transport of two scalars, for example the turbulent kinetic energy k and its dissipation ε. The Reynolds stress tensor is then computed using an assumption which relates the Reynolds stress tensor to the velocity gradients and an eddy viscosity. The latter is obtained from the two transported scalars.

IV. **Reynolds stress models.** Here a transport equation is derived for the Reynolds tensor $\overline{u_i u_j}$. One transport equation has to be added for determining the length scale of the turbulence. Usually an equation for the dissipation ε is used.

Above the different types of turbulence models have been listed in increasing order of complexity, ability to model the turbulence, and cost in terms of computational work (CPU time).

2.2   Boussinesq Assumption

In eddy viscosity turbulence models the Reynolds stresses are linked to the velocity gradients via the turbulent viscosity: this relation is called the Boussinesq assumption, where the Reynolds stress tensor in the time averaged Navier-Stokes equation is replaced by the turbulent viscosity multiplied by the velocity gradients. To show this we introduce this assumption for the diffusion term at the right-hand side of Eq. 2.6 and make an identification

$$\left[\mu(\bar{U}_{i,j} + \bar{U}_{j,i}) - \rho\overline{u_i u_j} \right]_{,j} = \left[(\mu + \mu_t)(\bar{U}_{i,j} + \bar{U}_{j,i}) \right]_{,j}$$

which gives

$$\rho\overline{u_i u_j} = -\mu_t(\bar{U}_{i,j} + \bar{U}_{j,i}). \tag{2.9}$$

If we in Eq. 2.9 do a contraction (i.e. setting indices $i = j$) the right-hand side gives

$$\overline{u_i u_i} \equiv 2k$$

where k is the turbulent kinetic energy (see Eq. 1.10). On the other hand the continuity equation (Eq. 2.5) gives that the right-hand side of Eq. 2.9

is equal to zero. In order to make Eq. 2.9 valid upon contraction we add $2/3\rho\delta_{ij}k$ to the left-hand side of Eq. 2.9 so that

$$\rho\overline{u_i u_j} = -\mu_t(\bar{U}_{i,j} + \bar{U}_{j,i}) + \frac{2}{3}\delta_{ij}\rho k. \tag{2.10}$$

Note that contraction of δ_{ij} gives

$$\delta_{ii} = \delta_{11} + \delta_{22} + \delta_{33} = 1 + 1 + 1 = 3$$

2.3 Algebraic Models

In eddy viscosity models we want an expression for the turbulent viscosity $\mu_t = \rho\nu_t$. The dimension of ν_t is $[\text{m}^2/\text{s}]$ (same as ν). A turbulent velocity scale multiplied with a turbulent length scale gives the correct dimension, i.e. **Eddy viscosity model**

$$\nu_t \propto \mathcal{U}\ell \tag{2.11}$$

Above we have used $\mathcal{U}$ and ℓ which are characteristic for the large turbulent scales. This is reasonable, because it is these scales which are responsible for most of the transport by turbulent diffusion.

In an algebraic turbulence model the velocity gradient is used as a velocity scale and some physical length is used as the length scale. In boundary layer-type of flow (see Eq. 2.7) we obtain

$$\nu_t = \ell_{mix}^2 \left| \frac{\partial U}{\partial y} \right| \tag{2.12}$$

where y is the coordinate normal to the wall, and where ℓ_{mix} is the mixing length, and the model is called the mixing length model. It is an old model and is hardly used any more. One problem with the model is that ℓ_{mix} is unknown and must be determined.

More modern algebraic models are the Baldwin-Lomax model [2] and the Cebeci-Smith [6] model which are frequently used in aerodynamics when computing the flow around airfoils, aeroplanes, etc. For a presentation and discussion of algebraic turbulence models the interested reader is referred to Wilcox [48].

2.4 Equations for Kinetic Energy

2.4.1 The Exact k Equation

The equation for turbulent kinetic energy $k = \frac{1}{2}\overline{u_i u_i}$ is derived from the Navier-Stokes equation which reads assuming steady, incompressible, constant viscosity (cf. Eq. 2.4)

$$(\rho U_i U_j)_{,j} = -P_{,i} + \mu U_{i,jj}. \tag{2.13}$$

The time averaged Navier-Stokes equation reads (cf. Eq. 2.6)

$$(\rho \bar{U}_i \bar{U}_j)_{,j} = -\bar{P}_{,i} + \mu \bar{U}_{i,jj} - \rho(\overline{u_i u_j})_{,j} \tag{2.14}$$

Subtract Eq. 2.14 from Eq. 2.13, multiply by u_i and time average and we obtain

$$\overline{\left[\rho U_i U_j - \rho \bar{U}_i \bar{U}_j\right]_{,j} u_i} =$$
$$-\overline{\left[P - \bar{P}\right]_{,i} u_i} + \mu \overline{\left[U_i - \bar{U}_i\right]_{,jj} u_i} + \rho \overline{(\overline{u_i u_j})_{,j} u_i} \tag{2.15}$$

The left-hand side can be rewritten as

$$\rho \overline{\left[(\bar{U}_i + u_i)(\bar{U}_j + u_j) - \bar{U}_i \bar{U}_j\right]_{,j} u_i} = \rho \overline{\left[\bar{U}_i u_j + u_i \bar{U}_j + u_i u_j\right]_{,j} u_i}. \tag{2.16}$$

Using the continuity equation $(\rho u_j)_{,j} = 0$, the first term is rewritten as

$$\overline{\left(\rho \bar{U}_i u_j\right)_{,j} u_i} = \rho \overline{u_i u_j} \bar{U}_{i,j}. \tag{2.17}$$

We obtain the second term (using $(\rho \bar{U}_j)_{,j} = 0$) from

$$\overline{\left(\rho \bar{U}_j k\right)_{,j}} = \bar{U}_j \rho \overline{\left[\frac{1}{2} u_i u_i\right]_{,j}} =$$
$$\frac{1}{2} \rho \bar{U}_j \overline{\{u_i u_{i,j} + u_i u_{i,j}\}} = \overline{u_i \left(\rho \bar{U}_j u_i\right)_{,j}} \tag{2.18}$$

The third term in Eq. 2.16 can be written as (using the same technique as in Eq. 2.18)

$$\frac{1}{2} \overline{(\rho u_j u_i u_i)_{,j}}. \tag{2.19}$$

The first term on the right-hand side of Eq. 2.15 has the form

$$-\overline{p_{,i} u_i} = -(\overline{p u_i})_{,i} \tag{2.20}$$

The second term on the right-hand side of Eq. 2.15 reads

$$\mu \overline{u_{i,jj} u_i} = \mu \left\{\overline{(u_{i,j} u_i)_{,j}} - \overline{u_{i,j} u_{i,j}}\right\} \tag{2.21}$$

For the first term we use the same trick as in Eq. 2.18 so that

$$\mu \overline{(u_{i,j} u_i)_{,j}} = \mu \frac{1}{2} \overline{(u_i u_i)_{,jj}} = \mu k_{,jj} \tag{2.22}$$

The last term on the right-hand side of Eq. 2.15 is zero. Now we can assemble the transport equation for the turbulent kinetic energy. Equations 2.17, 2.18, 2.20, 2.21, 2.22 give

$$\underbrace{(\rho \bar{U}_j k)_{,j}}_{I} = \underbrace{-\rho \overline{u_i u_j} \bar{U}_{i,j}}_{II} - \underbrace{\left[\overline{u_j p} + \frac{1}{2} \rho \overline{u_j u_i u_i} - \mu k_{,j}\right]_{,j}}_{III} - \underbrace{\mu \overline{u_{i,j} u_{i,j}}}_{IV} \tag{2.23}$$
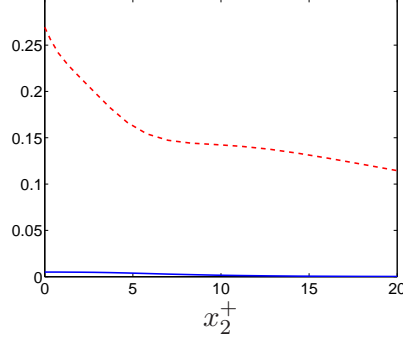
The terms in Eq. 2.23 have the following meaning.

Figure 2.3: Channel flow at $Re_\tau = 2000$. Comparison of mean and fluctuating dissipation terms. Both terms are normalized by u_τ^4/ν. DNS data [21, 20]. Solid line: $\nu(\partial \bar{V}_1/\partial x_2)^2$; dashed line: ε.

   I. Convection.

  II. Production. The large turbulent scales extract energy from the mean flow. This term (including the minus sign) is almost always positive.

 III. The two first terms represent **turbulent diffusion** by pressure-velocity fluctuations, and velocity fluctuations, respectively. The last term is viscous diffusion.

 IV. Dissipation. This term is responsible for transformation of kinetic energy at small scales to internal energy. The term (including the minus sign) is always negative.

In boundary-layer flow the exact k equation read

$$\frac{\partial \rho \bar{U} k}{\partial x} + \frac{\partial \rho \bar{V} k}{\partial y} = -\rho \overline{uv} \frac{\partial \bar{U}}{\partial y} - \frac{\partial}{\partial y} \left[\overline{pv} + \frac{1}{2} \overline{\rho v u_i u_i} - \mu \frac{\partial k}{\partial y} \right] - \mu \overline{u_{i,j} u_{i,j}} \quad (2.24)$$

Note that the dissipation includes all derivatives. This is because the dissipation term is at its largest for small, isotropic scales where the usual boundary-layer approximation that $\partial u_i/\partial x \ll \partial u_i/\partial y$ is not valid.

2.4.2 The Equation for $1/2(\bar{U}_i \bar{U}_i)$

The equation for $1/2(\bar{U}_i \bar{U}_i)$ is derived in the same way as that for $1/2\overline{u'_i u'_i}$. Assume steady, incompressible flow with constant viscosity and multiply the time-averaged Navier-Stokes equations (Eq. 2.14) so that

$$\bar{U}_i(\rho \bar{U}_i \bar{U}_j)_{,j} = -\bar{U}_i \bar{P}_{,i} + \mu \bar{U}_i \bar{U}_{i,jj} - \bar{U}_i \rho (\overline{u_i u_j})_{,j}. \quad (2.25)$$

The term on the left-hand side can be rewritten as

$$(\rho \bar{U}_i \bar{U}_i \bar{U}_j)_{,j} - \rho \bar{U}_i \bar{U}_j \bar{U}_{i,j} = \rho \bar{U}_j (\bar{U}_i \bar{U}_i)_{,j} - \frac{1}{2} \rho \bar{U}_j (\bar{U}_i \bar{U}_i)_{,j}$$

$$= \frac{1}{2} \rho \bar{U}_j (\bar{U}_i \bar{U}_i)_{,j} = (\rho \bar{U}_j \bar{K} K)_{,j} \quad (2.26)$$

The first term on the right-hand side of Eq. 2.25 can be written as

$$-U_i P_{,i} = -(U_i P)_{,i}. \tag{2.27}$$

The viscous term in Eq. 2.25 is rewritten in the same way as the viscous term in Section 2.4.1, see Eqs. 2.21 and 2.22, i.e.

$$\mu \bar{U}_i \bar{U}_{i,jj} = \mu \bar{K}_{,jj} - \mu \bar{U}_{i,j} \bar{U}_{i,j}. \tag{2.28}$$

Now we can assemble the transport equation for $\bar{K}$ by inserting Eqs. 2.26, 2.27 and 2.28 into Eq. 2.25

$$(\rho \bar{U}_j \bar{K})_{,j} = \mu \bar{K}_{,jj} - (\bar{U}_i \bar{P})_{,i} - \mu \bar{U}_{i,j} \bar{U}_{i,j} - \bar{U}_i \rho(\overline{u_i u_j})_{,j}, \tag{2.29}$$

where $\bar{K} = 1/2(\bar{U}_i \bar{U}_i)$. The last term is rewritten as

$$-\bar{U}_i \rho(\overline{u_i u_j})_{,j} = -(\bar{U}_i \rho \overline{u_i u_j})_{,j} + \rho(\overline{u_i u_j})\bar{U}_{i,j}. \tag{2.30}$$

Inserted in Eq. 2.29 gives

$$\begin{aligned}(\rho \bar{U}_j \bar{K})_{,j} = {} &\mu \bar{K}_{,jj} - (\bar{U}_i \bar{P})_{,i} - \mu \bar{U}_{i,j} \bar{U}_{i,j} \\ &- (\bar{U}_i \rho \overline{u_i u_j})_{,j} + \rho \overline{u_i u_j} \bar{U}_{i,j}.\end{aligned} \tag{2.31}$$

On the left-hand side we have the usual convective term. On the right-hand side we find: transport by viscous diffusion, transport by pressure-velocity interaction, viscous dissipation, transport by velocity-stress interaction and loss of energy to the fluctuating velocity field, i.e. to k. Note that the last term in Eq. 2.31 is the same as the last term in Eq. 2.23 but with opposite sign: here we clearly can see that the main source term in the k equation (the production term) appears as a sink term in the $\bar{K}$ equation.

In the $\bar{K}$ equation the dissipation term and the negative production term (representing loss of kinetic energy to the k field) read

$$-\mu \bar{U}_{i,j} \bar{U}_{i,j} + \rho \overline{u_i u_j} \bar{U}_{i,j}, \tag{2.32}$$

and in the k equation the production and the dissipation terms read

$$-\rho \overline{u_i u_j} \bar{U}_{i,j} - \mu \overline{u_{i,j} u_{i,j}}. \tag{2.33}$$

The gradient of the time-averaged velocity field, $\bar{U}_i$, is much smoother than that of the fluctuating velocity field, u_i'. Hence the dissipation by the fluctuations, ε, is much larger than the dissipation by the mean flow (left side of Eq. 2.32). This is clearly seen in Fig. 2.3. The mean dissipation, $\nu(\partial \bar{U}_1/\partial x_2)^2$, is largest at the wall where it takes the value $\nu = 1/2000$ (normalized by u_τ^4/ν).

2.5 The Modelled k Equation

In Eq. 2.23 a number of terms are unknown, namely the production term, the turbulent diffusion term and the dissipation term.

In the production term it is the stress tensor which is unknown. Since **production** we have an expression for this which is used in the Navier-Stokes equation **term** we use the same expression in the production term. Equation 2.10 inserted in the production term (term II) in Eq. 2.23 gives

$$P_k = -\rho \overline{u_i u_j} \bar{U}_{i,j} = \mu_t \left(\bar{U}_{i,j} + \bar{U}_{j,i} \right) \bar{U}_{i,j} - \frac{2}{3} \rho k \bar{U}_{i,i} \tag{2.34}$$

Note that the last term in Eq. 2.34 is zero for incompressible flow due to continuity.

The triple correlations in term III in Eq. 2.23 is modeled using a gradient **turbulent** law where we assume that k is diffused *down* the gradient, i.e from region of **diffusion** high k to regions of small k (cf. Fourier's law for heat flux: heat is diffused **term** from hot to cold regions). We get

$$\frac{1}{2} \overline{\rho u_j u_i u_i} = -\frac{\mu_t}{\sigma_k} k_{,j}. \tag{2.35}$$

where σ_k is the turbulent Prandtl number for k. There is no model for the pressure diffusion term in Eq. 2.23. It is small (see Figs. 4.1 and 4.3) and thus it is simply neglected.

The dissipation term in Eq. 2.23 is basically estimated as in Eq. 1.12. The **dissipation** velocity scale is now **term**

$$\mathcal{U} = \sqrt{k} \tag{2.36}$$

so that

$$\varepsilon \equiv \nu \overline{u_{i,j} u_{i,j}} = \frac{k^{\frac{3}{2}}}{\ell} \tag{2.37}$$

The modelled k equation can now be assembled and we get

$$(\rho \bar{U}_j k)_{,j} = \left[\left(\mu + \frac{\mu_t}{\sigma_k} \right) k_{,j} \right]_{,j} + P_k - \rho \frac{k^{\frac{3}{2}}}{\ell} \tag{2.38}$$

We have one constant in the turbulent diffusion term and it will be determined later. The dissipation term contains another unknown quantity, the turbulent length scale. An additional transport will be derived from which we can compute ℓ. In the $k - \varepsilon$ model, where ε is obtained from its own transport, the dissipation term $\rho k^{\frac{3}{2}}/\ell$ in Eq. 2.38 is simply $\rho \varepsilon$.

For boundary-layer flow Eq. 2.38 has the form

$$\frac{\partial \rho \bar{U} k}{\partial x} + \frac{\partial \rho \bar{V} k}{\partial y} = \frac{\partial}{\partial y} \left[\left(\mu + \frac{\mu_t}{\sigma_k} \right) \frac{\partial k}{\partial y} \right] + \mu_t \left(\frac{\partial \bar{U}}{\partial y} \right)^2 - \rho \frac{k^{\frac{3}{2}}}{\ell}. \tag{2.39}$$

2.6   One Equation Models

In one equation models a transport equation is often solved for the turbulent kinetic energy. The unknown turbulent length scale must be given, and often an algebraic expression is used [4, 50]. This length scale is, for example, taken as proportional to the thickness of the boundary layer, the width of a jet or a wake. The main disadvantage of this type of model is that it is not applicable to general flows since it is not possible to find a general expression for an algebraic length scale.

However, some proposals have been made where the turbulent length scale is computed in a more general way [14, 32]. In [32] a transport equation for turbulent viscosity is used.

3   Two-Equation Turbulence Models

3.1   The Modelled ε Equation

An exact equation for the dissipation can be derived from the Navier-Stokes equation (see, for instance, Wilcox [48]). However, the number of unknown terms is very large and they involve double correlations of fluctuating velocities, and gradients of fluctuating velocities and pressure. It is better to derive an ε equation based on physical reasoning. In the exact equation for ε the production term includes, as in the k equation, turbulent quantities and and velocity gradients. If we choose to include $\overline{u_i u_j}$ and $\bar{U}_{i,j}$ in the production term and only turbulent quantities in the dissipation term, we take, glancing at the k equation (Eq. 2.38)

$$P_\varepsilon \;\; = \;\; -c_{\varepsilon 1}\frac{\varepsilon}{k}\left(\bar{U}_{i,j}+\bar{U}_{j,i}\right)\bar{U}_{i,j} \tag{3.1}$$

$$\text{diss.term} \;\; = \;\; -c_{\varepsilon 2}\rho\frac{\varepsilon^2}{k}.$$

Note that for the production term we have $P_\varepsilon = c_{\varepsilon 1}(\varepsilon/k)P_k$. Now we can write the transport equation for the dissipation as

$$(\rho\bar{U}_j\varepsilon)_{,j} = \left[\left(\mu+\frac{\mu_t}{\sigma_\varepsilon}\right)\varepsilon_{,j}\right]_{,j} + \frac{\varepsilon}{k}\left(c_{\varepsilon 1}P_k - c_{\varepsilon 2}\rho\varepsilon\right) \tag{3.2}$$

For boundary-layer flow Eq. 3.2 reads

$$\frac{\partial\rho\bar{U}\varepsilon}{\partial x} + \frac{\partial\rho\bar{V}\varepsilon}{\partial y} = \frac{\partial}{\partial y}\left[\left(\mu+\frac{\mu_t}{\sigma_\varepsilon}\right)\frac{\partial\varepsilon}{\partial y}\right] + c_{\varepsilon 1}\frac{\varepsilon}{k}\mu_t\left(\frac{\partial\bar{U}}{\partial y}\right)^2 - \rho c_{\varepsilon 2}\frac{\varepsilon^2}{k} \tag{3.3}$$

3.2   Wall Functions

The natural way to treat wall boundaries is to make the grid sufficiently fine so that the sharp gradients prevailing there are resolved. Often, when computing complex three-dimensional flow, that requires too much computer resources. An alternative is to *assume* that the flow near the wall behaves like a fully developed turbulent boundary layer and prescribe boundary conditions employing wall functions. The assumption that the flow near the wall has the characteristics of a that in a boundary layer if often not true at all. However, given a maximum number of nodes that we can afford to use in a computation, it is often preferable to use wall functions which allows us to use fine grid in other regions where the gradients of the flow variables are large.

In a fully turbulent boundary layer the production term and the dissipation term in the log-law region ($30 < y^+ < 100$) are much larger than the
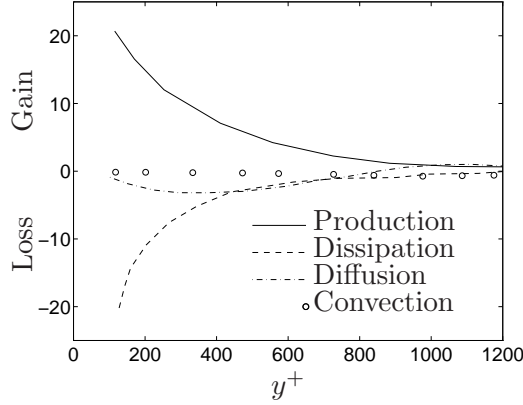
Figure 3.1: Boundary along a flat plate. Energy balance in k equation [45]. $Re_\delta \simeq 4400$, $u_*/U_0 \simeq 0.043$.

other terms, see Fig. 3.1. The log-law we use can be written as

$$\frac{U}{u_*} = \frac{1}{\kappa}\ln\left(\frac{Eu_*y}{\nu}\right) \tag{3.4}$$

$$E = 9.0 \tag{3.5}$$

Comparing this with the standard form of the log-law

$$\frac{U}{u_*} = A\ln\left(\frac{u_*y}{\nu}\right) + B \tag{3.6}$$

we see that

$$A = \frac{1}{\kappa}$$

$$\tag{3.7}$$

$$B = \frac{1}{\kappa}\ln E.$$

In the log-layer we can write the modelled k equation (see Eq. 2.39) as

$$0 = \mu_t\left(\frac{\partial\bar{U}}{\partial y}\right)^2 - \rho\varepsilon. \tag{3.8}$$

where we have replaced the dissipation term $\rho k^{\frac{3}{2}}/\ell$ by $\rho\varepsilon$. In the log-law region the shear stress $-\rho\overline{uv}$ is equal to the wall shear stress τ_w, see Fig. 2.1. The Boussinesq assumption for the shear stress reads (see Eq. 2.10)

$$\tau_w = -\rho\overline{uv} = \mu_t\frac{\partial\bar{U}}{\partial y} \tag{3.9}$$

Using the definition of the wall shear stress $\tau_w = \rho u_*^2$, and inserting Eqs. 3.9, 3.15 into Eq. 3.8 we get

$$c_\mu = \left(\frac{u_*^2}{k}\right)^2 \tag{3.10}$$

From experiments we have that in the log-law region of a boundary layer $u_*^2/k \simeq 0.3$ so that $c_\mu = 0.09$.

When we are using wall functions k and ε are not solved at the nodes adjacent to the walls. Instead they are fixed according to the theory presented above. The turbulent kinetic energy is set from Eq. 3.10, i.e.

$$k_P = c_\mu^{-1/2} u_*^2 \tag{3.11}$$

where the friction velocity u_* is obtained, iteratively, from the log-law (Eq. 3.4). Index P denotes the first interior node (adjacent to the wall).

The dissipation ε is obtained from observing that production and dissipation are in balance (see Eq. 3.8). The dissipation can thus be written as

$$\varepsilon_P = P_k = \frac{u_*^3}{\kappa y} \tag{3.12}$$

where the velocity gradient in the production term $-\overline{uv}\partial U/\partial y$ has been computed from the log-law in Eq. 3.4, i.e.

$$\frac{\partial U}{\partial y} = \frac{u_*}{\kappa y}. \tag{3.13}$$

For the velocity component parallel to the wall the wall shear stress is used as a flux boundary condition (cf. prescribing heat flux in the temperature equation).

When the wall is not parallel to any velocity component, it is more convenient to prescribe the turbulent viscosity. The wall shear stress τ_w is obtained by calculating the viscosity at the node adjacent to the wall from the log-law. The viscosity used in momentum equations is prescribed at the nodes adjacent to the wall (index P) as follows. The shear stress at the wall can be expressed as

$$\tau_w = \mu_{t,P}\frac{\partial \bar{U}}{\partial \eta} \approx \mu_{t,P}\frac{\bar{U}_{\|,P}}{\eta}$$

where $\bar{U}_{\|,P}$ denotes the velocity parallel to the wall and η is the normal distance to the wall. Using the definition of the friction velocity u_*

$$\tau_w = \rho u_*^2$$

we obtain

$$\mu_{t,P}\frac{\bar{U}_{\|,P}}{\eta} = \rho u_*^2 \rightarrow \mu_{t,P} = \frac{u_*}{\bar{U}_{\|,P}}\rho u_* \eta$$

Substituting $u_*/\bar{U}_{\|,P}$ with the log-law (Eq. 3.4) we finally can write

$$\mu_{t,P} = \frac{\rho u_* \eta \kappa}{\ln(E\eta^+)}$$

where $\eta^+ = u_*\eta/\nu$.

3.3 The $k - \varepsilon$ Model

In the $k - \varepsilon$ model the modelled transport equations for k and ε (Eqs. 2.38, 3.2) are solved. The turbulent length scale is obtained from (see Eq. 1.12, 2.37)

$$\ell = \frac{k^{3/2}}{\varepsilon}. \tag{3.14}$$

The turbulent viscosity is computed from (see Eqs. 2.11, 2.36, 1.12)

$$\nu_t = c_\mu k^{1/2} \ell = c_\mu \frac{k^2}{\varepsilon}. \tag{3.15}$$

We have five unknown constants $c_\mu, c_{\varepsilon 1}, c_{\varepsilon 2}, \sigma_k$ and σ_ε, which we hope should be universal i.e same for all types of flows. Simple flows are chosen where the equation can be simplified and where experimental data are used to determine the constants. The c_μ constant was determined above (Sub-section 3.2). The k equation in the logarithmic part of a turbulent boundary layer was studied where the convection and the diffusion term could be neglected.

In a similar way we can find a value for the $c_{\varepsilon 1}$ constant . We look at the ε equation for the logarithmic part of a turbulent boundary layer, where the convection term is negligible, and utilizing that production and dissipation are in balance $P_k = \rho \varepsilon$, we can write Eq. 3.3 as $\quad$ **$c_{\varepsilon 1}$ constant**

$$0 = \underbrace{\frac{\partial}{\partial y} \left[\frac{\mu_t}{\sigma_\varepsilon} \frac{\partial \varepsilon}{\partial y} \right]}_{D_\varepsilon} + (c_{\varepsilon 1} - c_{\varepsilon 2}) \rho \frac{\varepsilon^2}{k} \tag{3.16}$$

The dissipation and production term can be estimated as (see Sub-section 3.2)

$$\begin{aligned}
\varepsilon &= \frac{k^{3/2}}{\ell} \\
P_k &= \rho \frac{u_*^3}{\kappa y},
\end{aligned} \tag{3.17}$$

which together with $P_k = \rho \varepsilon$ gives

$$\ell = \kappa c_\mu^{-3/4} y. \tag{3.18}$$

In the logarithmic layer we have that $\partial k / \partial y = 0$, but from Eqs. 3.17, 3.18 we find that $\partial \varepsilon / \partial y \neq 0$. Instead the diffusion term in Eq. 3.16 can be rewritten using Eqs. 3.17, 3.18, 3.15 as

$$D_\varepsilon = \frac{\partial}{\partial y} \left[\frac{\mu_t}{\sigma_\varepsilon} \frac{\partial}{\partial y} \left(\frac{k^{3/2}}{\kappa c_\mu^{-3/4} y} \right) \right] = \frac{k^2 \kappa^2}{\sigma_\varepsilon \ell^2 c_\mu^{1/2}} \tag{3.19}$$

Inserting Eq. 3.19 and Eq. 3.17 into Eq. 3.16 gives

$$c_{\varepsilon 1} = c_{\varepsilon 2} - \frac{\kappa^2}{c_\mu^{1/2} \sigma_\varepsilon} \tag{3.20}$$

The flow behind a turbulence generating grid is a simple flow which allows us to determine the $c_{\varepsilon 2}$ constant. Far behind the grid the velocity gradients are very small which means that $P_k = 0$. Furthermore $V = 0$ and the diffusion terms are negligible so that the modelled k and ε equations (Eqs. 2.38, 3.2) read $\quad$ **$c_{\varepsilon 2}$ constant**

$$\rho \bar{U} \frac{dk}{dx} = -\rho \varepsilon \tag{3.21}$$

$$\rho \bar{U} \frac{d\varepsilon}{dx} = -c_{\varepsilon 2} \rho \frac{\varepsilon^2}{k} \tag{3.22}$$

Assuming that the decay of k is exponential $k \propto x^{-m}$, Eq. 3.21 gives $k \propto -mx^{-m-1}$. Insert this in Eq. 3.21, derivate to find $d\varepsilon/dx$ and insert it into Eq. 3.22 yields

$$c_{\varepsilon 2} = \frac{m+1}{m} \tag{3.23}$$

Experimental data give $m = 1.25 \pm 0.06$ [45], and $c_{\varepsilon 2} = 1.92$ is chosen.

We have found three relations (Eqs. 3.10, 3.20, 3.23) to determine three of the five unknown constants. The last two constants, σ_k and σ_ε, are optimized by applying the model to various fundamental flows such as flow in channel, pipes, jets, wakes, etc. The five constants are given the following values: $c_\mu = 0.09$, $c_{\varepsilon 1} = 1.44$, $c_{\varepsilon 2} = 1.92$, $\sigma_k = 1.0$, $\sigma_\varepsilon = 1.31$.

3.4 The $k - \omega$ Model

The $k - \omega$ model is gaining in popularity. The model was proposed by Wilcox [47, 48, 38]. In this model the standard k equation is solved, but as a length determining equation ω is used. This quantity is often called *specific dissipation* from its definition $\omega \propto \varepsilon/k$. The modelled k and ω equation read

$$(\rho \bar{U}_j k)_{,j} = \left[\left(\mu + \frac{\mu_t}{\sigma_k^\omega} \right) k_{,j} \right]_{,j} + P_k - \beta^* \omega k \tag{3.24}$$

$$(\rho \bar{U}_j \omega)_{,j} = \left[\left(\mu + \frac{\mu_t}{\sigma_\omega} \right) \omega_{,j} \right]_{,j} + \frac{\omega}{k} \left(c_{\omega 1} P_k - c_{\omega 2} \rho k \omega \right) \tag{3.25}$$

$$\mu_t = \rho \frac{k}{\omega}, \ \varepsilon = \beta^* \omega k.$$

The constants are determined as in Sub-section 3.3: $\beta^* = 0.09$, $c_{\omega 1} = 5/9$, $c_{\omega 2} = 3/40$, $\sigma_k^\omega = 2$ and $\sigma_\omega = 2$.

When wall functions are used k and ω are prescribed as (cf. Sub-section 3.2):

$$k_{wall} = (\beta^*)^{-1/2} u_*^2, \quad \omega_{wall} = (\beta^*)^{-1/2} \frac{u_*}{\kappa y}. \qquad (3.26)$$

In regions of low turbulence when both k and ε go to zero, large numerical problems for the $k - \varepsilon$ model appear in the ε equation as k becomes zero. The destruction term in the ε equation includes ε^2/k, and this causes problems as $k \to 0$ even if ε also goes to zero; they must both go to zero at a correct rate to avoid problems, and this is often not the case. On the contrary, no such problems appear in the ω equation. If $k \to 0$ in the ω equation in Eq. 3.24, the turbulent diffusion term simply goes to zero. Note that the production term in the ω equation does not include k since

$$\frac{\omega}{k} c_{\omega 1} P_k = \frac{\omega}{k} c_{\omega 1} \mu_t \left(\frac{\partial \bar{U}_i}{\partial x_j} + \frac{\partial \bar{U}_j}{\partial x_i} \right) \frac{\partial \bar{U}_i}{\partial x_j} = c_{\omega 1} \beta^* \left(\frac{\partial \bar{U}_i}{\partial x_j} + \frac{\partial \bar{U}_j}{\partial x_i} \right) \frac{\partial \bar{U}_i}{\partial x_j}.$$

In Ref. [37] the $k - \omega$ model was used to predict transitional, recirculating flow.

3.5 The $k - \tau$ Model

One of the most recent proposals is the $k - \tau$ model of Speziale *et al.* [41] where the transport equation for the turbulent time scale τ is derived. The exact equation for $\tau = k/\varepsilon$ is derived from the exact k and ε equations. The modelled k and τ equations read

$$(\rho \bar{U}_j k)_{,j} = \left[\left(\mu + \frac{\mu_t}{\sigma_k^\tau} \right) k_{,j} \right]_{,j} + P_k - \rho \frac{k}{\tau} \qquad (3.27)$$

$$\begin{aligned}
(\rho \bar{U}_j \tau)_{,j} &= \left[\left(\mu + \frac{\mu_t}{\sigma_{\tau 2}} \right) \tau_{,j} \right]_{,j} + \frac{\tau}{k} \left[(1 - c_{\varepsilon 1}) P_k + (c_{\varepsilon 2} - 1) \frac{k}{\tau} \right] (3.28) \\
&+ \frac{2}{k} \left(\mu + \frac{\mu_t}{\sigma_{\tau 1}} \right) k_{,j} \tau_{,j} - \frac{2}{\tau} \left(\mu + \frac{\mu_t}{\sigma_{\tau 2}} \right) \tau_{,j} \tau_{,j}
\end{aligned}$$

$$\mu_t = c_\mu \rho k \tau, \quad \varepsilon = k/\tau$$

The constants are: c_μ, $c_{\varepsilon 1}$ and $c_{\varepsilon 2}$ are taken from the $k - \varepsilon$ model, and $\sigma_k^\tau = \sigma_{\tau 1} = \sigma_{\tau 2} = 1.36$.

4 Low-Re Number Turbulence Models

In the previous section we discussed wall functions which are used in order to reduce the number of cells. However, we must be aware that this is an approximation which, if the flow near the boundary is important, can be rather crude. In many internal flows – where all boundaries are either walls, symmetry planes, inlet or outlets – the boundary layer may not be that important, as the flow field is often pressure-determined. For external flows (for example flow around cars, ships, aeroplanes etc.), however, the flow conditions in the boundaries are almost invariably important. When we are predicting heat transfer it is in general no good idea to use wall functions, because the heat transfer at the walls are very important for the temperature field in the whole domain.

When we chose not to use wall functions we thus insert sufficiently many grid lines near solid boundaries so that the boundary layer can be adequately resolved. However, when the wall is approached the viscous effects become more important and for $y^+ < 5$ the flow is viscous dominating, i.e. the viscous diffusion is much larger that the turbulent one (see Fig. 4.1). Thus, the turbulence models presented so far may not be correct since fully turbulent conditions have been assumed; this type of models are often referred to as high-Re number models. In this section we will discuss modifications of high-Re number models so that they can be used all the way down to the wall. These modified models are termed low Reynolds number models. Please note that "high Reynolds number" and "low Reynolds number" do *not* refer to the global Reynolds number (for example Re_L, Re_x, Re_x etc.) but here we are talking about the local turbulent Reynolds number $Re_\ell = \mathcal{U}\ell/\nu$ formed by a turbulent fluctuation and turbulent length scale. This Reynolds number varies throughout the computational domain and is proportional to the ratio of the turbulent and physical viscosity ν_t/ν, i.e. $Re_\ell \propto \nu_t/\nu$. This ratio is of the order of 100 or larger in fully turbulent flow and it goes to zero when a wall is approached.

We start by studying how various quantities behave close to the wall when $y \to 0$. Taylor expansion of the fluctuating velocities u_i (also valid for the mean velocities $\bar{U}_i$) gives

$$
\begin{aligned}
u &= a_0 + a_1 y + a_2 y^2 \ldots \\
v &= b_0 + b_1 y + b_2 y^2 \ldots \\
w &= c_0 + c_1 y + c_2 y^2 \ldots
\end{aligned}
\tag{4.1}
$$

where $a_0 \ldots c_2$ are functions of space and time. At the wall we have no-slip, i.e. $u = v = w = 0$ which gives $a_0 = b_0 = c_0$. Furthermore, at the wall $\partial u/\partial x = \partial w/\partial z = 0$, and the continuity equation gives $\partial v/\partial y = 0$ so that
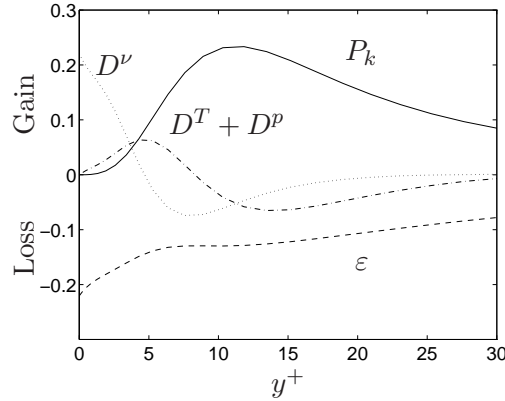
Figure 4.1: Flow between two parallel plates. Direct numerical simulations [23]. $Re = U_C\delta/\nu = 7890$. $u_*/U_C = 0.050$. Energy balance in k equation. Production P_k, dissipation ε, turbulent diffusion (by velocity triple correlations and pressure) $D^T + D^p$, and viscous diffusion D^ν. All terms have been scaled with u_*^4/ν.

$b_1 = 0$. Equation 4.1 can now be written

$$
\begin{aligned}
u &= a_1 y &+& a_2 y^2 \ldots \\
v &= && b_2 y^2 \ldots \\
w &= c_1 y &+& c_2 y^2 \ldots
\end{aligned}
\tag{4.2}
$$

From Eq. 4.2 we immediately get

$$
\begin{aligned}
\overline{u^2} &= \overline{a_1^2} y^2 \ldots & &= \mathcal{O}(y^2) \\
\overline{v^2} &= \overline{b_2^2} y^4 \ldots & &= \mathcal{O}(y^4) \\
\overline{w^2} &= \overline{c_1^2} y^2 \ldots & &= \mathcal{O}(y^2) \\
\overline{uv} &= \overline{a_1 b_2} y^3 \ldots & &= \mathcal{O}(y^3) \\
k &= \overline{(a_1^2 + c_1^2)} y^2 \ldots & &= \mathcal{O}(y^2) \\
\partial \bar{U}/\partial y &= \overline{a_1} \ldots & &= \mathcal{O}(y^0)
\end{aligned}
\tag{4.3}
$$

In Fig. 4.2 DNS-data for the fully developed flow in a channel is presented.

4.1 Low-Re $k - \varepsilon$ Models

There exist a number of Low-Re number $k - \varepsilon$ models [34, 7, 10, 1, 29]. When deriving low-Re models it is common to study the behavior of the terms when $y \to 0$ in the exact equations and require that the corresponding terms in the modelled equations behave in the same way. Let us study
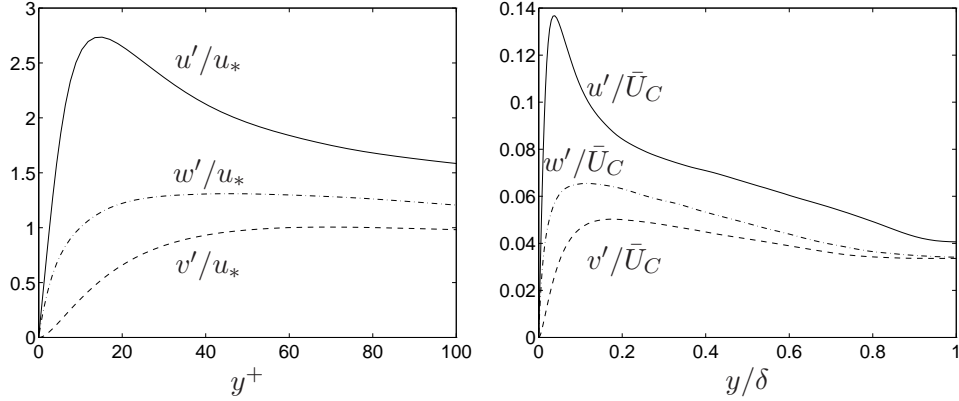
Figure 4.2: Flow between two parallel plates. Direct numerical simulations [23]. $Re = U_C \delta / \nu = 7890$. $u_* / U_C = 0.050$. Fluctuating velocity components $u'_i = \sqrt{\overline{u^2}_i}$.

the exact k equation near the wall (see Eq. 2.24).

$$\frac{\partial \rho \bar{U} k}{\partial x} + \frac{\partial \rho \bar{V} k}{\partial y} = \underbrace{-\rho \overline{uv} \frac{\partial \bar{U}}{\partial y}}_{\mathcal{O}(y^3)} - \frac{\partial \overline{pv}}{\partial y} \underbrace{- \frac{\partial}{\partial y} \left(\frac{1}{2} \overline{\rho v u_i u_i} \right)}_{\mathcal{O}(y^3)}$$
$$+ \mu \frac{\partial^2 k}{\partial y^2} - \underbrace{\mu \overline{u_{i,j} u_{i,j}}}_{\mathcal{O}(y^0)} \tag{4.4}$$

The pressure diffusion $\partial \overline{pv} / \partial y$ term is usually neglected, partly because it is not measurable, and partly because close to the wall it is not important, see Fig. 4.3 (see also [30]). The modelled equation reads

$$\frac{\partial \rho \bar{U} k}{\partial x} + \frac{\partial \rho \bar{V} k}{\partial y} = \underbrace{\mu_t \left(\frac{\partial \bar{U}}{\partial y} \right)^2}_{\mathcal{O}(y^4)} + \underbrace{\frac{\partial}{\partial y} \left(\frac{\mu_t}{\sigma_k} \frac{\partial k}{\partial y} \right)}_{\mathcal{O}(y^4)}$$
$$+ \mu \frac{\partial^2 k}{\partial y^2} - \underbrace{\rho \varepsilon}_{\mathcal{O}(y^0)} \tag{4.5}$$

When arriving at that the production term is $\mathcal{O}(y^4)$ we have used

$$\nu_t = c_\mu \rho \frac{k^2}{\varepsilon} = \frac{\mathcal{O}(y^4)}{\mathcal{O}(y^0)} = \mathcal{O}(y^4) \tag{4.6}$$

Comparing Eqs. 4.4 and 4.5 we find that the dissipation term in the modelled equation behaves in the same way as in the exact equation when
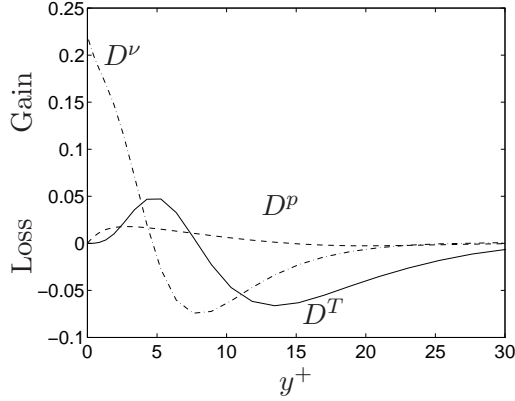
30

Figure 4.3: Flow between two parallel plates. Direct numerical simulations [23]. $Re = U_C \delta / \nu = 7890$. $u_* / U_C = 0.050$. Energy balance in k equation. Turbulent diffusion by velocity triple correlations D^T, Turbulent diffusion by pressure D^p, and viscous diffusion D^ν. All terms have been scaled with u_*^4 / ν.

$y \to 0$. However, both the modelled production and the diffusion term are of $\mathcal{O}(y^4)$ whereas the exact terms are of $\mathcal{O}(y^3)$. This inconsistency of the modelled terms can be removed by replacing the c_μ constant by $c_\mu f_\mu$ where f_μ is a damping function f_μ so that $f_\mu = \mathcal{O}(y^{-1})$ when $y \to 0$ and $f_\mu \to 1$ when $y^+ \geq 50$. Please note that the term "damping term" in this case is not correct since f_μ actually is augmenting μ_t when $y \to 0$ rather than damping. However, it is common to call all low-Re number functions for "damping functions".

Instead of introducing a damping function f_μ, we can choose to solve for a modified dissipation which is denoted $\tilde{\varepsilon}$, see Ref. [27] and Section 4.2.

It is possible to proceed in the same way when deriving damping functions for the ε equation [41]. An alternative way is to study the modelled ε equation near the wall and keep only the terms which do not tend to zero. From Eq. 3.3 we get

$$
\underbrace{\frac{\partial \rho \bar{U} \varepsilon}{\partial x}}_{\mathcal{O}(y^1)} + \underbrace{\frac{\partial \rho \bar{V} \varepsilon}{\partial y}}_{\mathcal{O}(y^1)} = \underbrace{c_{\varepsilon 1} \frac{\varepsilon}{k} P_k}_{\mathcal{O}(y^1)} + \underbrace{\frac{\partial}{\partial y} \left(\frac{\mu_t}{\sigma_\varepsilon} \frac{\partial \varepsilon}{\partial y} \right)}_{\mathcal{O}(y^1)}
$$
$$
+ \underbrace{\mu \frac{\partial^2 \varepsilon}{\partial y^2}}_{\mathcal{O}(y^0)} - \underbrace{c_{\varepsilon 2} \rho \frac{\varepsilon^2}{k}}_{\mathcal{O}(y^{-2})}
\tag{4.7}
$$

where it has been assumed that the production term P_k has been suitable modified so that $P_k = \mathcal{O}(y^3)$. We find that the only term which do not vanish at the wall are the viscous diffusion term and the dissipation term

so that close to the wall the dissipation equation reads

$$0 = \mu \frac{\partial^2 \varepsilon}{\partial y^2} - c_{\varepsilon 2} \rho \frac{\varepsilon^2}{k}. \tag{4.8}$$

The equation needs to be modified since the diffusion term cannot balance the destruction term when $y \to 0$.

4.2 The Launder-Sharma Low-Re $k - \varepsilon$ Models

There are at least a dozen different low Re $k - \varepsilon$ models presented in the literature. Most of them can be cast in the form [34] (in boundary-layer form, for convenience)

$$\frac{\partial \rho \bar{U} k}{\partial x} + \frac{\partial \rho \bar{V} k}{\partial y} = \frac{\partial}{\partial y} \left[\left(\mu + \frac{\mu_t}{\sigma_k} \right) \frac{\partial k}{\partial y} \right] + \mu_t \left(\frac{\partial \bar{U}}{\partial y} \right)^2 - \rho \varepsilon \tag{4.9}$$

$$\frac{\partial \rho \bar{U} \tilde{\varepsilon}}{\partial x} + \frac{\partial \rho \bar{V} \tilde{\varepsilon}}{\partial y} = \frac{\partial}{\partial y} \left[\left(\mu + \frac{\mu_t}{\sigma_\varepsilon} \right) \frac{\partial \tilde{\varepsilon}}{\partial y} \right] + c_{1\varepsilon} f_1 \frac{\tilde{\varepsilon}}{k} \mu_t \left(\frac{\partial \bar{U}}{\partial y} \right)^2$$
$$- c_{\varepsilon 2} f_2 \rho \frac{\tilde{\varepsilon}^2}{k} + E \tag{4.10}$$

$$\mu_t = c_\mu f_\mu \rho \frac{k^2}{\tilde{\varepsilon}} \tag{4.11}$$

$$\varepsilon = \tilde{\varepsilon} + D \tag{4.12}$$

Different models use different damping functions (f_μ, f_1 and f_2) and different extra terms (D and E). Many models solve for $\tilde{\varepsilon}$ rather than for ε where D is equal to the wall value of ε which gives an easy boundary condition $\tilde{\varepsilon} = 0$ (see Sub-section 4.3). Other models which solve for ε use no extra source in the k equation, i.e. $D = 0$.

Below we give some details for one of the most popular low-Re $k - \varepsilon$ models, the Launder-Sharma model [27] which is based on the model of **Launder-** Jones & Launder [22]. The model is given by Eqs. 4.9, 4.10, 4.11 and 4.12 **Sharma**

where

$$f_\mu = \exp\left(\frac{-3.4}{(1 + R_T/50)^2}\right)$$

$$f_1 = 1$$

$$f_2 = 1 - 0.3\exp\left(-R_T^2\right)$$

$$D = 2\mu\left(\frac{\partial\sqrt{k}}{\partial y}\right)^2 \tag{4.13}$$

$$E = 2\mu\frac{\mu_t}{\rho}\left(\frac{\partial^2\bar{U}}{\partial y^2}\right)^2$$

$$R_T = \frac{k^2}{\nu\tilde{\varepsilon}}$$

The term E was added to match the experimental peak in k around $y+ \simeq 20$ [22]. The f_2 term is introduced to mimic the final stage of decay of turbulence behind a turbulence generating grid when the exponent in $k \propto x^{-m}$ changes from $m = 1.25$ to $m = 2.5$.

4.3 Boundary Condition for ε and $\tilde{\varepsilon}$

In many low-Re $k - \varepsilon$ models $\tilde{\varepsilon}$ is the dependent variable rather than ε. The main reason is that the boundary condition for ε is rather complicated. The largest term in the k equation (see Eq. 4.4) close to the wall, are the dissipation term and the viscous diffusion term which both are of $\mathcal{O}(y^0)$ so that

$$0 = \mu\frac{\partial^2 k}{\partial y^2} - \rho\varepsilon. \tag{4.14}$$

From this equation we get immediately a boundary condition for ε as

$$\varepsilon_{wall} = \nu\frac{\partial^2 k}{\partial y^2}. \tag{4.15}$$

From Eq. 4.14 we can derive alternative boundary conditions. The exact form of the dissipation term close to the wall reads (see Eq. 2.24)

$$\varepsilon = \nu\overline{\left\{\left(\frac{\partial u}{\partial y}\right)^2 + \left(\frac{\partial w}{\partial y}\right)^2\right\}} \tag{4.16}$$

where $\partial/\partial y \gg \partial/\partial x \simeq \partial/\partial z$ and $u \simeq w \gg v$ have been assumed. Using Taylor expansion in Eq. 4.1 gives

$$\varepsilon = \nu\left(\overline{a_1^2} + \overline{c_1^2}\right) + \ldots \tag{4.17}$$

In the same way we get an expression for the turbulent kinetic energy

$$k = \frac{1}{2}\left(\overline{a_1^2} + \overline{c_1^2}\right) y^2 \dots \tag{4.18}$$

so that

$$\left(\frac{\partial \sqrt{k}}{\partial y}\right)^2 = \frac{1}{2}\left(\overline{a_1^2} + \overline{c_1^2}\right) \dots \tag{4.19}$$

Comparing Eqs. 4.17 and 4.19 we find

$$\varepsilon_{wall} = 2\nu \left(\frac{\partial \sqrt{k}}{\partial y}\right)^2. \tag{4.20}$$

In the Sharma-Launder model this is exactly the expression for D in Eqs. 4.12 and 4.13, which means that the boundary condition for $\tilde{\varepsilon}$ is zero, i.e. $\tilde{\varepsilon} = 0$.

In the model of Chien [8], the following boundary condition is used

$$\varepsilon_{wall} = 2\nu \frac{k}{y^2} \tag{4.21}$$

This is obtained by assuming $a_1 = c_1$ in Eqs. 4.17 and 4.18 so that

$$\begin{aligned} \varepsilon &= 2\nu \overline{a_1^2} \\ k &= \overline{a_1^2} y^2 \end{aligned} \tag{4.22}$$

which gives Eq. 4.21.

4.4 The Two-Layer $k - \varepsilon$ Model

Near the walls the one-equation model by Wolfshtein [50], modified by Chen and Patel [7], is used. In this model the standard k equation is solved; the diffusion term in the k-equation is modelled using the eddy viscosity assumption. The turbulent length scales are prescribed as [15, 11]

$$\ell_\mu = c_\ell n \left[1 - \exp\left(-R_n/A_\mu\right)\right], \ \ \ell_\varepsilon = c_\ell n \left[1 - \exp\left(-R_n/A_\varepsilon\right)\right]$$

(n is the normal distance from the wall) so that the dissipation term in the k-equation and the turbulent viscosity are obtained as:

$$\varepsilon = \frac{k^{3/2}}{\ell_\varepsilon}, \ \ \mu_t = c_\mu \rho \sqrt{k} \ell_\mu \tag{4.23}$$

The Reynolds number R_n and the constants are defined as

$$R_n = \frac{\sqrt{k}n}{\nu}, \ c_\mu = 0.09, \ c_\ell = \kappa c_\mu^{-3/4}, \ A_\mu = 70, \ A_\varepsilon = 2c_\ell$$

The one-equation model is used near the walls (for $R_n \leq 250$), and the standard high-Re $k - \varepsilon$ in the remaining part of the flow. The matching line could either be chosen along a pre-selected grid line, or it could be defined as the cell where the damping function

$$1 - \exp\left(-R_n/A_\mu\right)$$

takes, e.g., the value 0.95. The matching of the one-equation model and the $k - \varepsilon$ model does not pose any problems but gives a smooth distribution of μ_t and ε across the matching line.

4.5 The low-Re $k - \omega$ Model

A model which is being used more and more is the $k - \omega$ model of Wilcox [47]. The standard $k - \omega$ model can actually be used all the way to the wall without any modifications [47, 31, 36]. One problem is the boundary condition for ω at walls since (see Eq. 3.25)

$$\omega = \frac{\varepsilon}{\beta^* k} = \mathcal{O}(y^{-2}) \tag{4.24}$$

tends to infinity. In Sub-section 4.3 we derived boundary conditions for ε by studying the k equation close to the wall. In the same way we can here use the ω equation (Eq. 3.25) close to the wall to derive a boundary condition for ω. The largest terms in Eq. 3.25 are the viscous diffusion term and the destruction term, i.e.

$$0 = \mu \frac{\partial^2 \omega}{\partial y^2} - c_{\omega 2} \rho \omega^2. \tag{4.25}$$

The solution to this equation is

$$\omega = \frac{6\nu}{c_{\omega 2} y^2} \tag{4.26}$$

The ω equation is normally not solved close to the wall but for $y^+ < 2.5$, ω is computed from Eq. 4.26, and thus no boundary condition actually needed. This works well in finite volume methods but when finite element methods are used ω is needed *at* the wall. A slightly different approach must then be used [16].

Wilcox has also proposed a $k - \omega$ model [49] which is modified for viscous effects, i.e. a true low-Re model with damping function. He demonstrates that this model can predict transition and claims that it can be used for taking the effect of surface roughness into account which later has been confirmed [35]. A modification of this model has been proposed in [38].

4.5.1 The low-Re $k - \omega$ Model of Peng *et al.*

The $k - \omega$ model of Peng *et al.* reads [38]

$$\frac{\partial k}{\partial t} + \frac{\partial}{\partial x_j}(\bar{U}_j k) = \frac{\partial}{\partial x_j}\left[\left(\nu + \frac{\nu_t}{\sigma_k}\right)\frac{\partial k}{\partial x_j}\right] + P_k - c_k f_k \omega k$$

$$\frac{\partial \omega}{\partial t} + \frac{\partial}{\partial x_j}(\bar{U}_j \omega) = \frac{\partial}{\partial x_j}\left[\left(\nu + \frac{\nu_t}{\sigma_\omega}\right)\frac{\partial \omega}{\partial x_j}\right] + \frac{\omega}{k}\left(c_{\omega 1} f_\omega P_k - c_{\omega 2} k \omega\right) + c_\omega \frac{\nu_t}{k}\left(\frac{\partial k}{\partial x_j}\frac{\partial \omega}{\partial x_j}\right)$$

$$\nu_t = f_\mu \frac{k}{\omega}$$

$$f_k = 1 - 0.722 \exp\left[-\left(\frac{R_t}{10}\right)^4\right]$$

$$f_\mu = 0.025 + \left\{1 - \exp\left[-\left(\frac{R_t}{10}\right)^{3/4}\right]\right\}$$

$$\left\{0.975 + \frac{0.001}{R_t}\exp\left[-\left(\frac{R_t}{200}\right)^2\right]\right\}$$

$$f_\omega = 1 + 4.3\exp\left[-\left(\frac{R_t}{1.5}\right)^{1/2}\right],\ f_\omega = 1 + 4.3\exp\left[-\left(\frac{R_t}{1.5}\right)^{1/2}\right]$$

$$c_k = 0.09,\ c_{\omega 1} = 0.42,\ c_{\omega 2} = 0.075$$

$$c_\omega = 0.75, \sigma_k = 0.8,\ \sigma_\omega = 1.35$$

$$(4.27)$$

4.5.2 The low-Re $k - \omega$ Model of Bredberg *et al.*

A new $k - \omega$ model was recently proposed by Bredberg *et al.* [5] which reads

$$\frac{\partial k}{\partial t} + \frac{\partial}{\partial x_j}(\bar{U}_j k) = P_k - C_k k\omega + \frac{\partial}{\partial x_j}\left[\left(\nu + \frac{\nu_t}{\sigma_k}\right)\frac{\partial k}{\partial x_j}\right]$$

$$\frac{\partial \omega}{\partial t} + \frac{\partial}{\partial x_j}(\bar{U}_j \omega) = C_{\omega 1}\frac{\omega}{k}P_k - C_{\omega 2}\omega^2 + \qquad (4.28)$$

$$C_\omega\left(\frac{\nu}{k} + \frac{\nu_t}{k}\right)\frac{\partial k}{\partial x_j}\frac{\partial \omega}{\partial x_j} + \frac{\partial}{\partial x_j}\left[\left(\nu + \frac{\nu_t}{\sigma_\omega}\right)\frac{\partial \omega}{\partial x_j}\right]$$

The turbulent viscosity is given by

$$\nu_t = C_\mu f_\mu \frac{k}{\omega}$$

$$f_\mu = 0.09 + \left(0.91 + \frac{1}{R_t^3}\right)\left[1 - \exp\left\{-\left(\frac{R_t}{25}\right)^{2.75}\right\}\right] \qquad (4.29)$$

with the turbulent Reynolds number defined as $R_t = k/(\omega \nu)$. The constants in the model are given as

$$
\begin{aligned}
&C_k = 0.09, \quad C_\mu = 1, \quad C_\omega = 1.1, \quad C_{\omega 1} = 0.49, \\
&C_{\omega 2} = 0.072, \quad \sigma_k = 1, \quad \sigma_\omega = 1.8
\end{aligned}
\tag{4.30}
$$

5 Reynolds Stress Models

In Reynolds Stress Models the Boussinesq assumption (Eq. 2.10) is not used but a partial differential equation (transport equation) for the stress tensor is derived from the Navier-Stokes equation. This is done in the same way as for the k equation (Eq. 2.23).

Take the Navier-Stokes equation for the instantaneous velocity U_i (Eq. 2.4). Subtract the momentum equation for the time averaged velocity $\bar{U}_i$ ((Eq. 2.6) and multiply by u_j. Derive the same equation with indices i and j interchanged. Add the two equations and time average. The resulting equation reads

$$\underbrace{(\bar{U}_k \overline{u_i u_j})_{,k}}_{C_{ij}} = \underbrace{-\overline{u_i u_k} \bar{U}_{j,k} - \overline{u_j u_k} \bar{U}_{i,k}}_{P_{ij}} + \underbrace{\overline{\frac{p}{\rho}(u_{i,j} + u_{j,i})}}_{\Phi_{ij}}$$

$$\underbrace{- \left[\overline{u_i u_j u_k} + \frac{\overline{p u_j}}{\rho}\delta_{ik} + \frac{\overline{p u_i}}{\rho}\delta_{jk} - \nu(\overline{u_i u_j})_{,k} \right]_{,k}}_{D_{ij}} \qquad (5.1)$$

$$\underbrace{- 2\nu\overline{u_{i,k} u_{j,k}}}_{\varepsilon_{ij}}$$

where

P_{ij} is the production of $\overline{u_i u_j}$ [note that $P_{ii} = \frac{1}{2}P_k$ ($P_{ii} = P_{11} + P_{22} + P_{33}$)];

Φ_{ij} is the pressure-strain term, which promotes isotropy of the turbulence;

ε_{ij} is the dissipation (i.e. transformation of mechanical energy into heat in the small-scale turbulence) of $\overline{u_i u_j}$;

C_{ij} and D_{ij} are the convection and diffusion, respectively, of $\overline{u_i u_j}$.

Note that if we take the trace of Eq. 5.1 and divide by two we get the equation for the turbulent kinetic energy (Eq. 2.23). When taking the trace the pressure-strain term vanishes since

$$\Phi_{ii} = 2\overline{\frac{p}{\rho}u_{i,i}} = 0 \qquad (5.2)$$

due to continuity. Thus the pressure-strain term in the Reynolds stress equation does not add or destruct any turbulent kinetic energy it merely *redistributes* the energy between the normal components ($\overline{u^2}$, $\overline{v^2}$ and $\overline{w^2}$). Furthermore, it can be shown using physical reasoning [19] that Φ_{ij} acts to reduce the large normal stress component(s) and distributes this energy to the other normal component(s).

5.1   Reynolds Stress Models

We find that there are terms which are unknown in Eq. 5.1, such as the triple correlations $\overline{u_i u_j u_k}$, the pressure diffusion $(\overline{pu_j}\delta_{ik} + +\overline{pu_i}\delta_{jk})/\rho$ and the pressure strain Φ_{ij}, and the dissipation tensor ε_{ij}. From Navier-Stokes equation we could derive transport equations for this unknown quantities but this would add further unknowns to the equation system (the closure problem, see p. 12). Instead we supply models for the unknown terms.

The pressure strain term, which is an important term since its contribu- Φ_{ij}
tion is significant, is modelled as [26, 17]

$$\Phi_{ij} = \Phi_{ij,1} + \Phi_{ij,2} + \Phi'_{ij,1} + \Phi'_{ij,2}$$

$$\Phi_{ij,1} = -c_1\frac{\varepsilon}{k}\left(\overline{u_i u_j} - \frac{2}{3}\delta_{ij}k\right)$$

$$\Phi_{ij,2} = -c_2\left(P_{ij} - \frac{2}{3}\delta_{ij}P_k\right)$$

$$\Phi'_{nn,1} = -2c'_1\frac{\varepsilon}{k}\overline{u_n^2}f \qquad\qquad (5.3)$$

$$\Phi'_{ss,1} = c'_1\frac{\varepsilon}{k}\overline{u_n^2}f$$

$$f = \frac{k^{\frac{3}{2}}}{2.55x_n\varepsilon}$$

The object of the wall correction terms $\Phi'_{nn,1}$ and $\Phi'_{ss,1}$ is to take the effect of the wall into account. Here we have introduced a $s-n$ coordinate system, with s along the wall and n normal to the wall. Near a wall (the term "near" may well extend to $y^+ = 200$) the normal stress normal to the wall is damped (for a wall located at, for example, $x = 0$ this mean that the normal stress $\overline{v^2}$ is damped), and the other two are augmented (see Fig. 4.2).

In the literature there are many proposals for better (and more complicated) pressure strain models [42, 25].

The triple correlation in the diffusion term is often modelled as [9]   triple
                                                                           correla-
$$D_{ij} = \left(c_s\rho\overline{u_k u_m}\frac{k}{\varepsilon}(\overline{u_i u_j})_{,k}\right)_{,m} \qquad\qquad (5.4)$$ tion

The pressure diffusion term is for two reasons commonly neglected. First, it is not possible to measure this term and before DNS-data (Direct Numerical Simulations) were available it was thus not possible to model this term. Second, from DNS-data is has indeed been found to be small (see Fig. 4.3).

The dissipation tensor ε_{ij} is assumed to be isotropic, i.e.

$$\varepsilon_{ij} = \frac{2}{3}\delta_{ij}\varepsilon. \qquad\qquad (5.5)$$

From the definition of ε_{ij} (see 5.1) we find that the assumption in Eq. 5.5 is equivalent to assuming that for small scales (where dissipation occurs) the

two derivative $u_{i,k}$ and $u_{j,k}$ are not correlated for $i \neq j$. This is the same as assuming that for small scales u_i and u_j are not correlated for $i \neq j$ which is a good approximation since the turbulence at these small scale is isotropic, see Section 1.4.

We have given models for all unknown term in Eq. 5.1 and the *modelled* Reynolds equation reads [26, 17]

$$
\begin{aligned}
(\bar{U}_k \overline{u_i u_j})_{,k} = {} & -\overline{u_i u_k} \bar{U}_{j,k} - \overline{u_j u_k} \bar{U}_{i,k} \\
& + \left(\mu(\overline{u_i u_j})_{,k} + c_s \rho \overline{u_k u_m} \frac{k}{\varepsilon} (\overline{u_i u_j})_{,m} \right)_{,k} + \Phi_{ij} - \frac{2}{3} \delta_{ij} \rho \varepsilon
\end{aligned} \tag{5.6}
$$

where Φ_{ij} should be taken from Eq. 5.3. For a review on RSMs (<u>R</u>eynolds <u>S</u>tress <u>M</u>odels), see [18, 24, 28, 40].

5.2 Reynolds Stress Models *vs.* Eddy Viscosity Models

Whenever non-isotropic effects are *important* we should consider using RSMs. Note that in a turbulent boundary layer the turbulence is *always* non-isotropic, but isotropic eddy viscosity models handle this type of flow excellent as far as mean flow quantities are concerned. Of course a $k - \varepsilon$ model give very poor representation of the normal stresses. Examples where non-isotropic effects often are important are flows with strong curvature, swirling flows, flows with strong acceleration/retardation. Below we present list some advantages and disadvantages with RSMs and eddy viscosity models.

Advantages with eddy viscosity models:

i) simple due to the use of an isotropic eddy (turbulent) viscosity;
ii) stable via stability-promoting second-order gradients in the mean-flow equations;
iii) work reasonably well for a large number of engineering flows.

Disadvantages with eddy viscosity models:

i) isotropic, and thus not good in predicting normal stresses $(\overline{u^2}, \overline{v^2}, \overline{w^2})$;
ii) as a consequence of i) it is unable to account for curvature effects;
iii) as a consequence of i) it is unable to account for irrotational strains.

Advantages with RSMs:

i) the production terms need not to be modelled;
ii) thanks to i) it can selectively augment or damp the stresses due to curvature effects, acceleration/retardation, swirling flow, buoyancy etc.
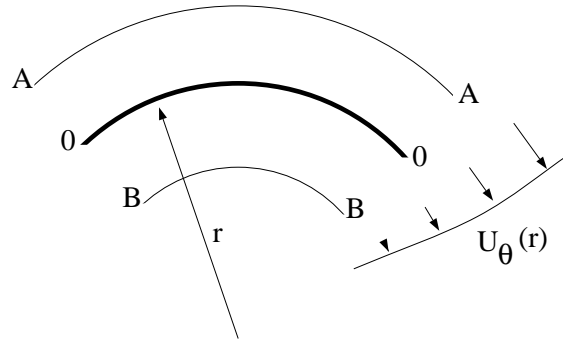
Disadvantages with RSMs:

Figure 5.1:   Curved boundary layer flow along $r = constant$. $U_\theta = U_\theta(r), U_r = 0$.

  i) complex and difficult to implement;
 ii) numerically unstable because small stabilizing second-order deriva-
     tives in the momentum equations (only <u>laminar</u> diffusion);
iii) CPU consuming.

5.3   Curvature Effects

Curvature effects, related either to curvature of the wall or streamline cur-
vature, are known to have significant effects on the turbulence [3]. Both
types of curvature are present in attached flows on curved surfaces, and
in separation regions. The entire Reynolds stress tensor is active in the
interaction process between shear stresses, normal stresses and mean ve-
locity strains. When predicting flows where curvature effects are impor-
tant, it is thus necessary to use turbulence models that accurately predict
all Reynolds stresses, not only the shear stresses. For a discussion of curva-
ture effects, see Refs. [12, 13].

    When the streamlines in boundary layer type of flow have a convex
(concave) curvature, the turbulence is stabilized (destabilized), which damp-
ens (augments) the turbulence [3, 39], especially the shear stress and the
Reynolds stress normal to the wall. Thus convex streamline curvature de-
creases the stress levels. It can be shown that it is the exact modelling of the
production terms in the RSM which allows the RSM to respond correctly to
this effect. The $k - \varepsilon$ model, in contrast, is not able to respond to streamline
curvature.

    The ratio of boundary layer thickness δ to curvature radius R is a com-
mon parameter for quantifying the curvature effects on the turbulence. The
work reviewed by Bradshaw demonstrates that even such small amounts
of convex curvature as $\delta/R = 0.01$ can have a significant effect on the tur-
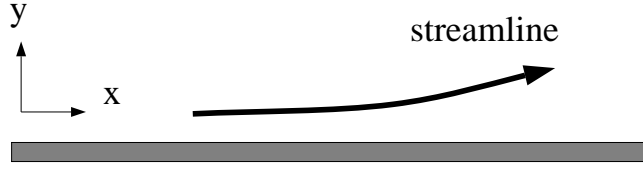bulence. Thompson and Whitelaw [44] carried out an experimental inves-

Figure 5.2: The streamlines which in flat-plate boundary layers are along the x-axis are suddenly deflected upwards (concave curvature) owing to e.g. an approaching separation region.

tigation on a configuration simulating the flow near a trailing edge of an airfoil, where they measured $\delta/R \simeq 0.03$. They reported a 50 percent decrease of $\rho\overline{v^2}$ (Reynolds stress in the normal direction to the wall) owing to curvature. The reduction of $\rho\overline{u^2}$ and $-\rho\overline{uv}$ was also substantial. In addition they reported significant damping of the turbulence in the shear layer in the outer part of the separation region.

An illustrative model case is curved boundary layer flow. A polar coordinate system $r - \theta$ (see Fig. 5.1)) with $\hat{\theta}$ locally aligned with the streamline is introduced. As $U_\theta = U_\theta(r)$ (with $\partial U_\theta/\partial r > 0$ and $U_r = 0$), the radial inviscid momentum equation degenerates to

$$\frac{\rho U_\theta^2}{r} - \frac{\partial p}{\partial r} = 0 \tag{5.7}$$

Here the variables are instantaneous or laminar. The centrifugal force exerts a force in the normal direction (outward) on a fluid following the streamline, which is balanced by the pressure gradient. If the fluid is displaced by some disturbance (e.g. turbulent fluctuation) outwards to level A, it encounters a pressure gradient larger than that to which it was accustomed at $r = r_0$, as $(U_\theta)_A > (U_\theta)_0$, which from Eq. 5.7 gives $(\partial p/\partial r)_A > (\partial p/\partial r)_0$. Hence the fluid is forced back to $r = r_0$. Similarly, if the fluid is displaced inwards to level B, the pressure gradient is smaller here than at $r = r_0$ and cannot keep the fluid at level B. Instead the centrifugal force drives it back to its original level.

It is clear from the model problem above that convex curvature, when $\partial U_\theta/\partial r > 0$, has a stabilizing effect on (turbulent) fluctuations, at least in the radial direction. It is discussed below how the Reynolds stress model responds to streamline curvature.

Assume that there is a flat-plate boundary layer flow. The ratio of the normal stresses $\rho\overline{u^2}$ and $\rho\overline{v^2}$ is typically 5. At one x station, the flow is deflected upwards, see Fig. 5.2. How will this affect the turbulence? Let us study the effect of concave streamline curvature. The production terms P_{ij} owing to rotational strains can be written as

	$\partial\bar{\mathbf{U}}_\theta/\partial\mathbf{r} > \mathbf{0}$	$\partial\bar{\mathbf{U}}_\theta/\partial\mathbf{r} < \mathbf{0}$
convex curvature	stabilizing	destabilizing
concave curvature	destabilizing	stabilizing

Table 5.1: *Effect of streamline curvature on turbulence.*

$$\text{RSM, } \overline{u^2} - \text{eq.} \quad : \qquad P_{11} = -2\rho\overline{uv}\frac{\partial\bar{U}}{\partial y} \tag{5.8}$$

$$\text{RSM, } \overline{uv} - \text{eq.} \quad : \qquad P_{12} = -\rho\overline{u^2}\frac{\partial\bar{V}}{\partial x} - \rho\overline{v^2}\frac{\partial\bar{U}}{\partial y} \tag{5.9}$$

$$\text{RSM, } \overline{v^2} - \text{eq.} \quad : \qquad P_{22} = -2\rho\overline{uv}\frac{\partial\bar{V}}{\partial x} \tag{5.10}$$

$$k - \varepsilon \quad : \qquad P_k = \mu_t\left(\frac{\partial\bar{U}}{\partial y} + \frac{\partial\bar{V}}{\partial x}\right)^2 \tag{5.11}$$

As long as the streamlines in Fig. 5.2 are parallel to the wall, all production is a result of $\partial\bar{U}/\partial y$. However as soon as the streamlines are deflected, there are more terms resulting from $\partial\bar{V}/\partial x$. Even if $\partial\bar{V}/\partial x$ is much smaller that $\partial\bar{U}/\partial y$ it will still contribute non-negligibly to P_{12} as $\rho\overline{u^2}$ is much larger than $\rho\overline{v^2}$. Thus the magnitude of P_{12} will increase (P_{12} is negative) as $\partial\bar{V}/\partial x > 0$. An increase in the magnitude of P_{12} will increase $-\overline{uv}$, which in turn will increase P_{11} and P_{22}. This means that $\rho\overline{u^2}$ and $\rho\overline{v^2}$ will be larger and the magnitude of P_{12} will be further increased, and so on. It is seen that there is a positive feedback, which continuously increases the Reynolds stresses. It can be said that the turbulence is *destabilized* owing to concave curvature of the streamlines.

However, the $k - \varepsilon$ model is not very sensitive to streamline curvature (neither convex nor concave), as the two rotational strains are multiplied by the same coefficient (the turbulent viscosity).

If the flow (concave curvature) in Fig. 5.2 is a wall jet flow where $\partial\bar{U}/\partial y < 0$, the situation will be reversed: the turbulence will be *stabilized*. If the streamline (and the wall) in Fig. 5.2 is deflected downwards, the situation will be as follows: the turbulence is stabilizing when $\partial\bar{U}/\partial y > 0$, and destabilizing for $\partial\bar{U}/\partial y < 0$.

The stabilizing or destabilizing effect of streamline curvature is thus dependent on the type of curvature (convex or concave), and whether there is an increase or decrease in momentum in the tangential direction with radial distance from its origin (i.e. the sign of $\partial\bar{U}_\theta/\partial r$). For convenience, these cases are summarized in Table 5.1.
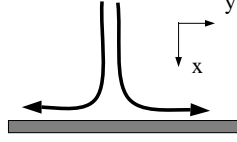
Figure 5.3: Stagnation flow.

5.4 Acceleration and Retardation

When the flow accelerates and/or decelerate the irrotational strains ($\partial \bar{U}/\partial x$, $\partial \bar{V}/\partial y$ and $\partial \bar{W}/\partial z$) become important.

In boundary layer flow, the only term which contributes to the production term in the k equation is $-\rho \overline{uv} \partial U/\partial y$ (x denotes streamwise direction). Thompson and Whitelaw [44] found that, near the separation point as well as in the separation zone, the production term $-\rho(\overline{u^2} - \overline{v^2})\partial U/\partial x$ is of equal importance. This was confirmed in prediction of separated flow using RSM [12, 13].

In pure boundary layer flow the only term which contributes to the production term in the k and ε-equations is $-\rho \overline{uv} \partial \bar{U}/\partial y$. Thompson and Whitelaw [44] found that near the separation point, as well as in the separation zone, the production term $-\rho(\overline{u^2} - \overline{v^2})\partial \bar{U}/\partial x$ is of equal importance. As the exact form of the production terms are used in second-moment closures, the production due to irrotational strains is correctly accounted for.

In the case of stagnation-like flow (see Fig. 5.3), where $\overline{u^2} \simeq \overline{v^2}$ the production due to normal stresses is zero, which is also the results given by second-moment closure, whereas $k - \varepsilon$ models give a large production. In order to illustrate this, let us write the production due to the irrotational strains $\partial \bar{U}/\partial x$ and $\partial \bar{V}/\partial y$ for RSM and $k - \varepsilon$:

$$RSM \quad : \quad 0.5\,(P_{11} + P_{22}) = -\rho \overline{u^2} \frac{\partial \bar{U}}{\partial x} - \rho \overline{v^2} \frac{\partial \bar{V}}{\partial y}$$

$$k - \varepsilon \quad : \quad P_k = 2\mu_t \left\{ \left(\frac{\partial \bar{U}}{\partial x} \right)^2 + \left(\frac{\partial \bar{V}}{\partial y} \right)^2 \right\}$$

If $\overline{u^2} \simeq \overline{v^2}$ we get $P_{11} + P_{22} \simeq 0$ since $\partial \bar{U}/\partial x = -\partial \bar{V}/\partial y$ due to continuity. The production term P_k in $k - \varepsilon$ model, however, will be large, since it will be *sum* of the two strains.

References

[1] ABE, K., KONDOH, T., AND NAGANO, Y. A new turbulence model for predicting fluid flow and heat transfer in separating and reattaching flows - 1. Flow field calculations. *Int. J. Heat Mass Transfer 37* (1994), 139–151.

[2] BALDWIN, B., AND LOMAX, H. Thin-layer approximation and algebraic model for separated turbulent flows. AIAA 78-257, Huntsville, AL, 1978.

[3] BRADSHAW, P. Effects of streamline curvature on turbulent flow. Agardograph progress no. 169, AGARD, 1973.

[4] BRADSHAW, P., FERRISS, D., AND ATWELL, N. Calculation of boundary-layer development using the turbulent energy equation. *Journal of Fluid Mechanics 28* (1967), 593–616.

[5] BREDBERG, J., PENG, S.-H., AND DAVIDSON, L. An improved $k - \omega$ turbulence model applied to recirculating flows. *International Journal of Heat and Fluid Flow 23*, 6 (2002), 731–743.

[6] CEBECI, T., AND SMITH, A. *Analysis of Turbulent Boundary Layers*. Academic Press, 1974.

[7] CHEN, H., AND PATEL, V. Near-wall turbulence models for complex flows including separation. *AIAA Journal 26* (1988), 641–648.

[8] CHIEN, K. Predictions of channel and boundary layer flows with a low-reynolds-number turbulence model. *AIAA Journal 20* (1982), 33–38.

[9] DALY, B., AND HARLOW, F. Transport equation in turbulence. *Physics of Fluids 13* (1970), 2634–2649.

[10] DAVIDSON, L. Calculation of the turbulent buoyancy-driven flow in a rectangular cavity using an efficient solver and two different low reynolds number $k - \varepsilon$ turbulence models. *Numer. Heat Transfer 18* (1990), 129–147.

[11] DAVIDSON, L. Reynolds stress transport modelling of shock/boundary-layer interaction. 24th AIAA Fluid Dynamics Conference, AIAA 93-3099, Orlando, 1993.

[12] DAVIDSON, L. Prediction of the flow around an airfoil using a Reynolds stress transport model. *Journal of Fluids Engineering 117* (1995), 50–57.

[13] DAVIDSON, L. Reynolds stress transport modelling of shock-induced separated flow. *Computers & Fluids 24* (1995), 253–268.

[14] DAVIDSON, L., AND OLSSON, E. Calculation of some parabolic and elliptic flows using a new one-equation turbulence model. In *5th Int. Conf. on Numerical Methods in Laminar and Turbulent Flow* (1987), C. Taylor, W. Habashi, and M. Hafez, Eds., Pineridge Press, pp. 411–422.

[15] DAVIDSON, L., AND RIZZI, A. Navier-Stokes stall predictions using an algebraic stress model. *J. Spacecraft and Rockets 29* (1992), 794–800.

[16] EMVIN, P. *The Full Multigrid Method Applied to Turbulent Flow in Ventilated Enclosures Using Structured and Unstructured Grids.* PhD thesis, Dept. of Thermo and Fluid Dynamics, Chalmers University of Technology, Göteborg, 1997.

[17] GIBSON, M., AND LAUNDER, B. Ground effects on pressure fluctuations in the atmospheric boundary layer. *Journal of Fluid Mechanics 86* (1978), 491–511.

[18] HANJALIĆ, K. Advanced turbulence closure models: A view of current status and future prospects. *Int. J. Heat and Fluid Flow 15* (1994), 178–203.

[19] HINZE, J. *Turbulence*, second ed. McGraw-Hill, New York, 1975.

[20] HOYAS, S., AND JIMÉNEZ, J. http://torroja.dmt.upm.es/ftp/channels/data/statistics/.

[21] HOYAS, S., AND JIMÉNEZ, J. Scaling of the velocity fluctuations in turbulent channels up to $Re_\tau = 2003$. *Physics of Fluids A 18*, 011702 (2006).

[22] JONES, W., AND LAUNDER, B. The prediction of laminarization with a two-equation model of turbulence. *Int. J. Heat Mass Transfer 15* (1972), 301–314.

[23] KIM, J. The collaborative testing of turbulence models (organized by P. Bradshaw *et al.*). Data Disk No. 4 (also available at Ercoftac's www-server http://fluindigo.mech.surrey.ac.uk/database), 1990.

[24] LAUNDER, B. Second-moment closure: Present ... and future? *Int. J. Heat and Fluid Flow 10* (1989), 282–300.

[25] LAUNDER, B., AND LI, S.-P. On the elimination of wall-topography parameters from second-moment closures. *Physics of Fluids A 6* (1994), 999–1006.

[26] LAUNDER, B., REECE, G., AND RODI, W. Progress in the development of a Reynolds-stress turbulence closure. *Journal of Fluid Mechanics 68*, 3 (1975), 537–566.

[27] LAUNDER, B., AND SHARMA, B. Application of the energy dissipation model of turbulence to the calculation of flow near a spinning disc. *Lett. Heat and Mass Transfer 1* (1974), 131–138.

[28] LESCHZINER, M. Modelling engineering flows with Reynolds stress turbulence closure. *J. Wind Engng. and Ind. Aerodyn. 35* (1991), 21–47.

[29] LIEN, F., AND LESCHZINER, M. Low-Reynolds-number eddy-viscosity modelling based on non-linear stress-strain/vorticity relations. In *Engineering Turbulence Modelling and Experiments 3* (1996), W. Rodi and G. Bergeles, Eds., Elsevier, pp. 91–100.

[30] MANSOUR, N., KIM, J., AND MOIN, P. Reynolds-stress and dissipation-rate budgets in a turbulent channel flow. *Journal of Fluid Mechanics 194* (1988), 15–44.

[31] MENTER, F. Two-equation eddy-viscosity turbulence models for engineering applications. *AIAA Journal 32* (1994), 1598–1605.

[32] MENTER, F. On the connection between one- and two-equation models of turbulence. In *Engineering Turbulence Modelling and Experiments 3* (1996), W. Rodi and G. Bergeles, Eds., Elsevier, pp. 131–140.

[33] PANTON, R. *Incompressible Flow*. John Wiley & Sons, New York, 1984.

[34] PATEL, V., RODI, W., AND SCHEUERER, G. Turbulence models for near-wall and low Reynolds number flows: A review. *AIAA Journal 23* (1985), 1308–1319.

[35] PATEL, V., AND YOON, J. Application of turbulence models to separated flows over rough surfaces. *Journal of Fluids Engineering 117* (1995), 234–241.

[36] PENG, S.-H., DAVIDSON, L., AND HOLMBERG, S. Performance of two-equation turbulence models for numerical simulation of ventilation flows. In *5th Int. Conf. on Air Distributions in Rooms, ROOMVENT'96* (Yokohama, Japan, 1996), S. Murakami, Ed., vol. 2, pp. 153–160.

[37] PENG, S.-H., DAVIDSON, L., AND HOLMBERG, S. The two-equations turbulence $k-\omega$ model applied to recirculating ventilation flows. Tech. Rep. 96/13, Dept. of Thermo and Fluid Dynamics, Chalmers University of Technology, Gothenburg, 1996.

[38] PENG, S.-H., DAVIDSON, L., AND HOLMBERG, S. A modified low-Reynolds-number $k - \omega$ model for recirculating flows. *Journal of Fluids Engineering 119* (1997), 867–875.

[39] RODI, W., AND SCHEUERER, G. Calculation of curved shear layers with two-equation turbulence models. *Physics of Fluids 26* (1983), 1422–1435.

[40] SO, R., LAI, Y., AND ZHANG, H. Second-order near-wall turbulence closures: a review. *AIAA Journal 29* (1991), 1819–1835.

[41] SPEZIALE, C., ABID, R., AND ANDERSON, E. Critical evaluation of two-equation models for near-wall turbulence. *AIAA Journal 30* (1992), 324–331.

[42] SPEZIALE, C., SARKAR, S., AND GATSKI, T. Modelling the pressure-strain correlation of turbulence: an invariant dynamical system approach. *Journal of Fluid Mechanics 227* (1991), 245–272.

[43] TENNEKES, H., AND LUMLEY, J. *A First Course in Turbulence*. The MIT Press, Cambridge, Massachusetts, 1972.

[44] THOMPSON, B., AND WHITELAW, J. Characteristics of a trailing-edge flow with turbulent boundary-layer separation. *Journal of Fluid Mechanics 157* (1985), 305–326.

[45] TOWNSEND, A. *The Structure of Turbulent Shear Flow*, second ed. Cambridge University Press, New York, 1976.

[46] WHITE, F. *Fluid Mechanics*. McGraw-Hill, Inc., New York, 1994.

[47] WILCOX, D. Reassessment of the scale-determining equation. *AIAA Journal 26*, 11 (1988), 1299–1310.

[48] WILCOX, D. *Turbulence Modeling for CFD*. DCW Industries, Inc., 5354 Palm Drive, La Cañada, California 91011, 1993.

[49] WILCOX, D. Simulation of transition with a two-equation turbulence model. *AIAA Journal 32* (1994), 247–255.

[50] WOLFSHTEIN, M. The velocity and temperature distribution in one-dimensional flow with turbulence augmentation and pressure gradient. *Int. J. Mass Heat Transfer 12* (1969), 301–318.